IEEE Access
Multidisciplinary | Rapid Review | Open Access Journal

Received September 5, 2020, accepted September 28, 2020, date of publication October 6, 2020, date of current version October 21, 2020.

*Digital Object Identifier 10.1109/ACCESS.2020.3028860*

# On the Performance of Full-Duplex Spatial Modulation MIMO System With and Without Transmit Antenna Selection Under Imperfect Hardware Conditions

**BA CAO NGUYEN[1], XUAN NAM TRAN[2], (Member, IEEE), LE VAN NGUYEN[2], AND LE THE DUNG[3,4], (Member, IEEE)**

[1]Faculty of Basic Techniques, Telecommunications University, Khanh Hoa 650000, Vietnam
[2]Faculty of Radio Electronics, Le Quy Don Technical University, Hanoi 23583, Vietnam
[3]Division of Computational Physics, Institute for Computational Science, Ton Duc Thang University, Ho Chi Minh City 758307, Vietnam
[4]Faculty of Electrical and Electronics Engineering, Ton Duc Thang University, Ho Chi Minh City 758307, Vietnam

Corresponding author: Le The Dung (lethedung@tdtu.edu.vn)

**ABSTRACT** Hardware impairments (HI) due to imperfect manufactured electronic parts degrade the performance of wireless systems. In this paper, we consider a bidirectional full-duplex (FD) spatial modulation (SM) multiple-input multiple-output (MIMO) system with non-ideal hardware and residual self-interference (RSI). We propose to use the transmission antenna selection (TAS) as a solution to mitigate this degradation. The performance of the considered system is analyzed using mathematical analysis. Specifically, we first derive the exact closed-form expressions of the outage probability (OP), symbol error probability (SEP), and achievable data rate (ADR) for two cases: with and without TAS. Given these expressions, we conduct a detailed evaluation of the system performance under various scenarios to gain insight into its behavior. Essential conclusions are then made on HI and RSI's impacts, especially for the case with TAS and high transmission rates.

**INDEX TERMS** Full-duplex, self-interference cancellation, spatial modulation, transmit antenna selection, hardware impairments, outage probability, symbol error probability, ergodic capacity.

## I. INTRODUCTION

Nowadays, the need for Internet-of-Things (IoT) devices has increased very fast to provide users with anytime and anywhere connection to the Internet [1], [2]. Different types of IoT devices have been developed to meet various requirements for health-care, automatic driving, smart home, and smart city applications [3], [4]. It is expected that there will be billions IoT devices to exchange data over a limited range of available frequencies. Spectrum efficiency is thus a prime concern for telecom service providers and frequency management authority. Meanwhile, there is an increasing requirement for transmission quality in the wireless broadband systems. Various technical solutions have been proposed to improve the spectrum efficiency such as full-duplex (FD), multiple-input multiple-output (MIMO), spatial modulation (SM), and non-orthogonal multiple access (NOMA) [1], [3].

Recently, there has been a great interest in conducting researches on FD and SM techniques for single user communications [5]–[7]. The in-band FD technique is a very effective solution for increasing frequency utilization as it allows for simultaneous transmission and reception over the same frequency band [4], [7]. The FD technique is also known as a promising solution for reducing feedback delay and end-to-end latency, increasing network secrecy, avoiding transmission collisions and the hidden terminal problem in wireless networks [4], [8]. Meanwhile, SM is a MIMO transmission technique with many important advantages for IoT applications. SM-MIMO systems use only a single antenna for transmission to avoid the inter-channel interference (ICI) and facilitate the inter-antenna synchronization (IAS) requirement. As only a single transmit radio frequency (RF) chain is required, reducing hardware complexity and saving energy

The associate editor coordinating the review of this manuscript and approving it for publication was Nizar Zorba.

consumption are possible. However, by using antenna shift keying according to the transmitted data, SM-MIMO systems can transmit more bits thanks to the combinations of different antenna indexes. With multiple receive antennas, these systems can still attain spatial diversity by using low-complexity iterative maximal-ratio combining (MRC) for signal estimation [5], [6], [9]. The advantage of combining FD and SM is thus a twofold, i.e., not only achieve spectral efficiency but also improve the performance of IoT systems. This has motivated various research efforts in FD-SM-MIMO systems [10]–[12].

One major concern in FD-SM-MIMO systems is the self-interference (SI) due to FD transmission mode. To make it possible for applications, different self-interference cancellation (SIC) techniques in propagation, analog, and digital domains has been applied into FD transmission mode. The analyses and experiments in the literature has demonstrated that SI can be suppressed up to 110 dB, which is similar to a noise level [13], [14]. Such residual SI (RSI) might not be accepted for applications that require high reliability as it still affects detection accuracy. Recent researches have addressed the impacts of RSI in various published works [10], [15], [16]. Another concern not only for the FD-SM-MIMO system but also typical wireless transceivers is hardware impairments (HI). Due to imperfect manufactured electronic parts, especially low-cost devices, HI such as high-power amplifier (HPA) nonlinearity, phase noise (PN) and in-phase/quadrature (I/Q) imbalance often cause a mismatch between the desired and actual signals. Although manufacturers try to reduce the HI as much as possible during manufacturing processes, they still exist as the inherent issues of all electronic devices. Various techniques have been proposed to tackle these impairments in both analog and digital domains [17]–[20]. However, recent researches still considered the existence of the residual impairments in transmitters and receivers as independent additive noise sources [17], [18]. It was shown that HI can reduce the system capacity and increase the outage probability (OP) and symbol error rate (SER) of the wireless systems [17]. Moreover, HI were also shown to cause imperfect SIC in FD devices [14] and reduce the performance of high data rate systems [17], [18], [20]. Therefore, for FD-SM-MIMO systems, neglecting HI while analyzing the performance of these systems may result in insufficient evaluations and conclusions.

In a recent research, the work in [10] investigated the possibility of combining FD and SM in a $2\times2$ MIMO system. It was shown that the FD-SM-MIMO system could achieve higher capacity than the half-duplex (HD)-SM-MIMO system with a small performance loss in outage and SER probability. The later work in [11] considered the application of FD-SM in a two-way relay system in order to increase the system throughput. The paper has obtained the mathematical expressions for pairwise error probability (PEP) and upper bound bit error probability of the system. The analytical results show a strong impact of RSI on the performance of the FD-SM two-way relay system. Using both FD and SM at the relay, the authors of [12] considered an FD-SM-MIMO cooperative system which has the direct link from the source to the destination. The work has derived the mathematical expressions for the average error probability and the achievable rate of the system under the presence of RSI. The subsequent works in [15], [16] also evaluated the performance of the FD-SM-MIMO cooperative systems with FD-SM relays. They have derived the upper-bound BER for the case with energy harvesting (EH) at the FD relay [16] and the OP for the cascaded $\alpha-\mu$ fading channel [15]. Recently, the researches on FD-SM-MIMO systems continuously increase due to the benefits of FD, SM and MIMO techniques [21]–[23]. In the future, FD-SM-MIMO systems can be successfully deployed for various applications such as IoT, device-to-device (D2D) and vehicle-to-vehicle (V2V) communications.

Recently, the impacts of HI and RSI have been considered for the FD-SM-MIMO system in the case of relaying [24]. The authors in [24] investigated a TAS-SM-FDR system and demonstrated that both HI and RSI have a strong influence on the OP and SER of the system. However, the achievable data rate (ADR) was not studied. Although some expressions in [24] can be used for a point-to-point system with HI and RSI, certain influences of HI and RSI need to be investigated further. Specifically, [24] only considered some cases of specific values of HI and RSI, the case of both HI and RSI simultaneously change was not investigated. Moreover, despite the fact that effective cancellation solutions were used there still exist residual interference sources due to SI and HI. This motivates us to find a simple yet effective solution to enhance the performance of the FD-SM-MIMO system to compensate for the joint impact of both HI and RSI. Specifically, we consider the transmit antenna selection (TAS), which was proposed for the SM-MIMO systems [24]–[26], for the FD-SM-MIMO system and analyze its performance to have an insight into its behaviors under various conditions. Note that, TAS can alleviate the effect of RSI and HI on the system performance indirectly. Specifically, by applying TAS at the transmitter, the received signal power at the receiver is significantly enhanced in comparison with the case without TAS [26]. Therefore, the effects of negative factors such as RSI, HI, and Gaussian noise are reduced in the HI-FD-SM-MIMO system. Unlike previous reports, we successfully obtain the exact closed-form mathematical expressions of OP, SEP, and ADR of the considered HI-FD-SM-MIMO system with and without TAS. From our results, the OP, SEP, and ADR of SM-MIMO system with perfect hardware and perfect SIC can be easily derived. Additionally, so far, this is the first work obtaining three mathematical expressions (OP, SEP, and ADR) of the SM-MIMO system under the joint and cross effects of HI and RSI in the cases with and without TAS.

The main contributions of this paper are summarized as follows:

- We propose to use TAS as an effective solution to compensate for the joint impact of both HI and RSI in a point-to-point FD-SM-MIMO system over the Rayleigh fading channel. Unlike [24], in this paper, HI and RSI

are simultaneously changed for investigating the system performance. Additionally, the ADR, an important metric to evaluate the system performance, is provided.

- We first derive the signal-to-interference-plus-noise and distortion ratio (SINDR) and then use it to derive the exact closed-form expressions of OP, SEP and ADR of the considered system in the case of perfect antenna index estimation. Our derived expressions can be conveniently applied to other related systems such as the ideal-hardware FD-SM-MIMO system (hereafter referred to as the ideal-FD-SM-MIMO system), the ideal-HD-SM-MIMO system, and the HI-HD-SM-MIMO one.
- The impact of HI and RSI on the system's OP, throughput, SEP, and ADR especially for the high rate system, under various practical scenarios are analyzed using numerical calculations. The efficacy of TAS is also evaluated versus the case without TAS. Recommendations are then drawn for setting up FD-SM-MIMO systems with the best performance.

The rest of this paper is organized as follows. Section II describes the system and signal model of the considered HI-FD-SM-MIMO system. Section III presents detailed derivations of the mathematical expressions of the OP, SEP, and ADR. Numerical results and discussions are provided in Section IV. Finally, Section V concludes the paper.

## II. SYSTEM MODEL

Fig. 1 illustrates the system model of the HI-FD-SM-MIMO system. Two terminals, denoted by A and B, exchange their data with each other using FD mode. Terminal A has $N_{\mathrm{tA}}$ transmission antennas and $N_{\mathrm{rA}}$ reception antennas. Meanwhile, B has $N_{\mathrm{tB}}$ transmission antennas and $N_{\mathrm{rB}}$ reception antennas. There is the self-interference (SI) from transmission to the reception antennas, which distorts the received signal. Although shared-antennas can be used at the two terminals together with a circulator, in this paper, we use separate transmission and reception antennas for better SI suppression [13], [27], [28]. Specifically, the work in [28] demonstrated that the shared-antennas is difficult in configuration because of the significant crosstalk between them. Since the distance between the transmission and reception antennas of a terminal is short, the power of SI signals is very high. Therefore, all possible SIC techniques in the propagation, analog and digital domains should be applied to achieve the best SI suppression. First, SI is suppressed during the signal propagation by jointly using antenna directionality, path loss, and cross-polarization [28]. Then, in the analog and digital domains, SI is canceled by using analog cancellation circuits and digital signal processing [28], [29].

In the case of ideal hardware, the received signals at A and B are, respectively, expressed as

$$\mathbf{y}_{\mathrm{A}} = \mathbf{h}_{j\mathrm{A}} x_j + \mathbf{h}_{i\mathrm{A}} x_i + \mathbf{z}_{\mathrm{A}}, \quad (1)$$

$$\mathbf{y}_{\mathrm{B}} = \mathbf{h}_{i\mathrm{B}} x_i + \mathbf{h}_{j\mathrm{B}} x_j + \mathbf{z}_{\mathrm{B}}, \quad (2)$$

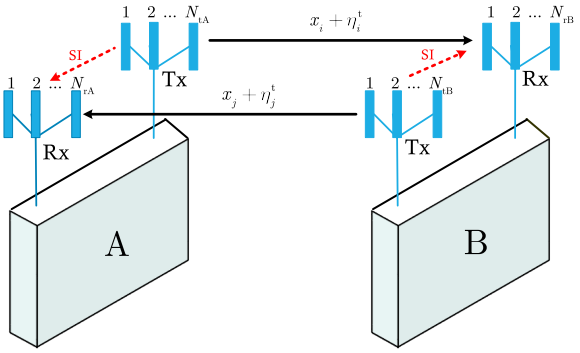


**FIGURE 1.** System model of the considered FD-SM-MIMO system with hardware impairments and self-interference.

where $\mathbf{h}_{i\mathrm{A}}$ and $\mathbf{h}_{j\mathrm{A}}$ are respectively the channel vectors from the $i$th transmission antenna of A and from the $j$th transmission antenna of B to $N_{\mathrm{rA}}$ reception antennas of A; $\mathbf{h}_{i\mathrm{B}}$ and $\mathbf{h}_{j\mathrm{B}}$ are respectively the channel vectors from the $i$th transmission antenna of A and from the $j$th transmission antenna of B to $N_{\mathrm{rB}}$ reception antennas of B; $i = 1, 2, \ldots, N_{\mathrm{tA}}$ and $j = 1, 2, \ldots, N_{\mathrm{tB}}$; $x_i$ and $x_j$ are the transmitted signals from the $i$th antenna of A and the $j$th antenna of B, respectively; $\mathbf{z}_{\mathrm{A}}$ and $\mathbf{z}_{\mathrm{B}}$ denote respectively the Gaussian noise vectors at A and B with zero mean and variance of $\sigma^2$, i.e. $\mathbf{z}_{\mathrm{A}} \sim \mathcal{CN}(0, \sigma_{\mathrm{A}}^2)$ and $\mathbf{z}_{\mathrm{B}} \sim \mathcal{CN}(0, \sigma_{\mathrm{B}}^2)$.

In realistic systems, due to imperfect manufacturing of electronic parts, especially in low-cost devices, hardware impairments such as phase noise (PN), in-phase/quadrature (I/Q) imbalance and nonlinearities of various components such as analog-to-digital (A/D) and digital-to-analog (D/A) converters, mixers and amplifiers (high power amplifier (HPA) in the transmitter and the low-noise amplifier (LNA) in the receiver) often cause the mismatch between the desired and actual signals [17]–[19], [30]–[32]. Various techniques have been proposed to tackle these impairments in both analog and digital domains [17]–[19], [33], [34]. Specifically, PN is mitigated via an estimation and compensation approach based on maximum-likelihood theory [19]. I/Q imbalances at both the transmitter and receiver are suppressed by using different data-aided estimation and compensation approaches [19], [31], [34]. The nonlinearities of components can be mitigated by using highly linear components [19], [32], [34]. However, distortion noises cannot be completely removed due to the residual impairments caused by the intrinsic defect of electronic components, the imperfect parameter estimation of random and time varying hardware characteristics, the inaccuracy coming from limited precision models, unsophisticated compensation algorithms, etc. Furthermore, all impairments are time-dependent because they take new realizations for each new data signal [18], [19]. Based on central limit theorem and experiments, the aggregate effect from many impairments can be modeled by complex Gaussian variables with zero mean and finite variance [17], [18], [30].

The received signals at terminals A and B in the case of hardware impairments can be expressed as follows

$$\mathbf{y}_{\mathrm{A}} = \mathbf{h}_{j\mathrm{A}}(x_j + \eta_j^{\mathrm{t}}) + \mathbf{h}_{i\mathrm{A}}(x_i + \eta_i^{\mathrm{t}}) + \boldsymbol{\eta}_{\mathrm{A}}^{\mathrm{r}} + \mathbf{z}_{\mathrm{A}}, \quad (3)$$

$$\mathbf{y}_{\mathrm{B}} = \mathbf{h}_{i\mathrm{B}}(x_i + \eta_i^{\mathrm{t}}) + \mathbf{h}_{j\mathrm{B}}(x_j + \eta_j^{\mathrm{t}}) + \boldsymbol{\eta}_{\mathrm{B}}^{\mathrm{r}} + \mathbf{z}_{\mathrm{B}}, \quad (4)$$

where $\eta_i^{\mathrm{t}}$ and $\eta_j^{\mathrm{t}}$ denote the distortion noises caused by the transmitter hardware impairments at A and B, respectively; $\boldsymbol{\eta}_{\mathrm{A}}^{\mathrm{r}}$ and $\boldsymbol{\eta}_{\mathrm{B}}^{\mathrm{r}}$ are the distortion noise vectors caused by the receiver hardware impairments at A and B, respectively. It is also noted that, after signal processing, the residual hardware impairments follow the Gaussian distributions [17], [18], [24], i.e., $\eta_i^{\mathrm{t}} \sim \mathcal{CN}(0, (k_{\mathrm{A}}^{\mathrm{t}})^2 P_{\mathrm{A}})$ and $\eta_j^{\mathrm{t}} \sim \mathcal{CN}(0, (k_{\mathrm{B}}^{\mathrm{t}})^2 P_{\mathrm{B}})$, where $k_{\mathrm{A}}^{\mathrm{t}}$ and $k_{\mathrm{B}}^{\mathrm{t}}$ denote the levels of HI at the transmitters of A and B, respectively. At the receivers, we get $\boldsymbol{\eta}_{\mathrm{A}}^{\mathrm{r}} \sim \mathcal{CN}(0, (k_{\mathrm{A}}^{\mathrm{r}})^2 P_{\mathrm{B}} \|\mathbf{h}_{j\mathrm{A}}\|^2)$ and $\boldsymbol{\eta}_{\mathrm{B}}^{\mathrm{r}} \sim \mathcal{CN}(0, (k_{\mathrm{B}}^{\mathrm{r}})^2 P_{\mathrm{A}} \|\mathbf{h}_{i\mathrm{B}}\|^2)$, where $k_{\mathrm{A}}^{\mathrm{r}}$ and $k_{\mathrm{B}}^{\mathrm{r}}$ denote the levels of HI at receivers A and B, respectively.

As shown in (3) and (4), the terms $\mathbf{h}_{i\mathrm{A}}(x_i + \eta_i^{\mathrm{t}})$ and $\mathbf{h}_{j\mathrm{B}}(x_j + \eta_j^{\mathrm{t}})$ are the SI at terminals A and B, which need to be suppressed. Upon application of all possible SIC techniques the residual self-interference (RSI) at A and B, denoted by $\mathbf{r}_{\mathrm{SI_A}}$ and $\mathbf{r}_{\mathrm{SI_B}}$ respectively, become complex Gaussian distributed random variables [7], [14], [35] with zero mean and variances of $\sigma^2_{\mathrm{RSI}}$, i.e. $\sigma^2_{\mathrm{RSI_A}} = l_{\mathrm{A}}^2 P_{\mathrm{A}}$ and $\sigma^2_{\mathrm{RSI_B}} = l_{\mathrm{B}}^2 P_{\mathrm{B}}$. Here $l_{\mathrm{A}}$ and $l_{\mathrm{B}}$ denote the SIC capability of A and B; $P_{\mathrm{A}}$ and $P_{\mathrm{B}}$ are the average transmission power of A and B, respectively.

The received signals at A and B after SIC can be now expressed as follows

$$\mathbf{y}_{\mathrm{A}} = \mathbf{h}_{j\mathrm{A}}(x_j + \eta_j^{\mathrm{t}}) + \mathbf{r}_{\mathrm{SI_A}} + \boldsymbol{\eta}_{\mathrm{A}}^{\mathrm{r}} + \mathbf{z}_{\mathrm{A}}, \quad (5)$$

$$\mathbf{y}_{\mathrm{B}} = \mathbf{h}_{i\mathrm{B}}(x_i + \eta_i^{\mathrm{t}}) + \mathbf{r}_{\mathrm{SI_B}} + \boldsymbol{\eta}_{\mathrm{B}}^{\mathrm{r}} + \mathbf{z}_{\mathrm{B}}, \quad (6)$$

where the channel vectors $\mathbf{h}_{j\mathrm{A}}$ and $\mathbf{h}_{i\mathrm{B}}$ are given by

$$\mathbf{h}_{j\mathrm{A}} = \begin{bmatrix} h_{j1} & h_{j2} & \dots & h_{jN_{\mathrm{rA}}} \end{bmatrix}, \quad (7)$$

$$\mathbf{h}_{i\mathrm{B}} = \begin{bmatrix} h_{i1} & h_{i2} & \dots & h_{iN_{\mathrm{rB}}} \end{bmatrix}, \quad (8)$$

with $i = 1, 2, \dots, N_{\mathrm{tA}}$ and $j = 1, 2, \dots, N_{\mathrm{tB}}$.

Upon application of SM, depending on the incoming data bits, only one antenna is activated for transmission. For example, with two transmission antennas, the first one is activated for transmitting "0" bit, while the second one transmitting "1" bit. When TAS is applied in the SM-MIMO system, the sets of $S_{\mathrm{A}}$ and $S_{\mathrm{B}}$ transmission antennas are first selected from the $N_{\mathrm{tA}}$ and $N_{\mathrm{tB}}$ transmission antennas at A and B, respectively. Then, one transmission antenna is activated from each set for the signal transmission. The sets $S_{\mathrm{A}}$ and $S_{\mathrm{B}}$ must satisfy the conditions: $S_{\mathrm{A}} \leq N_{\mathrm{tA}}, S_{\mathrm{A}} = 2^m$, and $S_{\mathrm{B}} \leq N_{\mathrm{tB}}, S_{\mathrm{B}} = 2^n$ with $m$ and $n$ being positive integers. Furthermore, $S_{\mathrm{A}}$ and $S_{\mathrm{B}}$ are selected such that the received signal power at the receivers is maximized. For example, when $|S_{\mathrm{A}}| = 2$ and the norms of channel vector $\mathbf{h}_{i\mathrm{B}}$ satisfy the following condition

$$\|\mathbf{h}_{1\mathrm{B}}\|^2 \geq \|\mathbf{h}_{2\mathrm{B}}\|^2 \geq \|\mathbf{h}_{3\mathrm{B}}\|^2 \geq \ldots \geq \|\mathbf{h}_{N_{\mathrm{tA}}\mathrm{B}}\|^2, \quad (9)$$

the set $S_{\mathrm{A}}$ is computed as

$$S_{\mathrm{A}} = \{\|\mathbf{h}_{1\mathrm{B}}\|^2, \|\mathbf{h}_{2\mathrm{B}}\|^2\}. \quad (10)$$

It is noted that if the incoming bit is "0", the first antenna is activated. Otherwise, the second antenna is activated. In addition, besides the norm-based TAS as presented in this paper, other TAS schemes such as capacity optimized antenna selection (COAS) [25] and Euclidean distance optimized antenna selection (EDAS) [25], [36] can be exploited for the considered system to achieve higher performance. However, compared with the TAS, the computational complexities of EDAS method and its variations are significantly higher. On the other hand, although COAS has lower complexity than EDAS, it still needs further processing compared to the norm-based TAS. For this TAS, the objective function is only included the channel power gain, which has been estimated in our system. In terms of maximizing the signal power to improve the system capacity, the norm-based TAS scheme is somehow similar to the COAS scheme. Furthermore, since all SIC techniques are applied at A and B, the signal processing complexity at them is already high. Therefore, we applied norm-based TAS for the considered HI-FD-SM-MIMO system to significantly reduce the computational complexity but can keep the performance as close to alternative methods as possible.

At the receiver side, maximal ratio combining (MRC) is used to coherently combine the signals from $N_{\mathrm{r}}$ reception antennas ($N_{\mathrm{rA}}$ at terminal A and $N_{\mathrm{rB}}$ at terminal B). Then, to recover the transmitted bits, the receiver can use joint maximum likelihood (ML) detection for estimating both activated transmit antenna index and $M_o$-ary modulated symbols. In this paper, as we are interested in analyzing the impact of both HI and RSI as well as the effect of the TAS scheme on the system performance, we assume that the receivers of both A and B can perfectly estimate the activated antenna indices of respective transmitters for the ML detection. This assumption may not fully reflect the behavior of practical SM system. However, as reported in [15], [22], [25], [37]–[39], this assumption helps to significantly reduce the computational complexity in calculating while it causes slight error in comparison with the case of imperfect estimation the activated antenna index [22], [38], [39]. As can be seen from Fig. 3 of [38], in low SNR (SNR $\leq -10$ dB) and high SNR (SNR $\geq 20$ dB), there is no antenna detection error, the upper and lower bounds converge to the simulated capacity. Moreover, since we apply TAS for the considered system with the presence of both HI and RSI, the mathematical derivations are very complex. Therefore, it is reasonable to assume that the correct information of transmit antenna indices is alway available at the receivers.

From the received signals in (5) and (6), the SINDRs at terminal A, $\gamma_{\mathrm{A}}$, and terminal B, $\gamma_{\mathrm{B}}$, are given by

$$\gamma_{\mathrm{A}} = \frac{\|\mathbf{h}_{j\mathrm{A}}\|^2 P_{\mathrm{B}}}{\|\mathbf{h}_{j\mathrm{A}}\|^2 (k_{\mathrm{B}}^{\mathrm{t}})^2 P_{\mathrm{B}} + (k_{\mathrm{A}}^{\mathrm{r}})^2 P_{\mathrm{B}} \|\mathbf{h}_{j\mathrm{A}}\|^2 + \sigma^2_{\mathrm{RSI_A}} + \sigma_{\mathrm{A}}^2}. \quad (11)$$

$$\gamma_{\mathrm{B}} = \frac{\|\mathbf{h}_{i\mathrm{B}}\|^2 P_{\mathrm{A}}}{\|\mathbf{h}_{i\mathrm{B}}\|^2 (k_{\mathrm{A}}^{\mathrm{t}})^2 P_{\mathrm{A}} + (k_{\mathrm{B}}^{\mathrm{r}})^2 P_{\mathrm{A}} \|\mathbf{h}_{i\mathrm{B}}\|^2 + \sigma^2_{\mathrm{RSI_B}} + \sigma^2_{\mathrm{B}}}. \quad (12)$$

Let $k_{\mathrm{A}}^2 = (k_{\mathrm{B}}^{\mathrm{t}})^2 + (k_{\mathrm{A}}^{\mathrm{r}})^2$ and $k_{\mathrm{B}}^2 = (k_{\mathrm{A}}^{\mathrm{t}})^2 + (k_{\mathrm{B}}^{\mathrm{r}})^2$ be the aggregate distortions, where $k_{\mathrm{A}}$ is the aggregate impairment level which accounts for that in both transmitter B ($k_{\mathrm{B}}^{\mathrm{t}}$) and receiver A ($k_{\mathrm{A}}^{\mathrm{r}}$); $k_{\mathrm{B}}$ is the aggregate impairment level which accounts for that in both transmitter A ($k_{\mathrm{A}}^{\mathrm{t}}$) and receiver B ($k_{\mathrm{B}}^{\mathrm{r}}$). As a result, (11) and (12) become

$$\gamma_{\mathrm{A}} = \frac{\|\mathbf{h}_{j\mathrm{A}}\|^2 P_{\mathrm{B}}}{\|\mathbf{h}_{j\mathrm{A}}\|^2 k_{\mathrm{A}}^2 P_{\mathrm{B}} + \sigma^2_{\mathrm{RSI_A}} + \sigma^2_{\mathrm{A}}} = \frac{\|\mathbf{h}_{j\mathrm{A}}\|^2 \bar{\gamma}_{\mathrm{A}}}{\|\mathbf{h}_{j\mathrm{A}}\|^2 k_{\mathrm{A}}^2 \bar{\gamma}_{\mathrm{A}} + 1}, \quad (13)$$

$$\gamma_{\mathrm{B}} = \frac{\|\mathbf{h}_{i\mathrm{B}}\|^2 P_{\mathrm{A}}}{\|\mathbf{h}_{i\mathrm{B}}\|^2 k_{\mathrm{B}}^2 P_{\mathrm{A}} + \sigma^2_{\mathrm{RSI_B}} + \sigma^2_{\mathrm{B}}} = \frac{\|\mathbf{h}_{i\mathrm{B}}\|^2 \bar{\gamma}_{\mathrm{B}}}{\|\mathbf{h}_{i\mathrm{B}}\|^2 k_{\mathrm{B}}^2 \bar{\gamma}_{\mathrm{B}} + 1}, \quad (14)$$

where

$$\bar{\gamma}_{\mathrm{A}} = \frac{P_{\mathrm{B}}}{\sigma^2_{\mathrm{RSI_A}} + \sigma^2_{\mathrm{A}}}, \text{ and } \bar{\gamma}_{\mathrm{B}} = \frac{P_{\mathrm{A}}}{\sigma^2_{\mathrm{RSI_B}} + \sigma^2_{\mathrm{B}}}$$

denote the average SINR at A and B, respectively.

It can be clearly seen from (13) and (14) that the SINDRs at the receivers depend on the terms $\|\mathbf{h}_{i\mathrm{B}}\|^2$ and $\|\mathbf{h}_{j\mathrm{A}}\|^2$. Thus, to improve the system performance, it is crucially necessary to increase $\|\mathbf{h}_{i\mathrm{B}}\|^2$ and $\|\mathbf{h}_{j\mathrm{A}}\|^2$. In this context, TAS is a good solution because it can maximize $\|\mathbf{h}_{i\mathrm{B}}\|^2$ and $\|\mathbf{h}_{j\mathrm{A}}\|^2$. In addition, the signal-to-noise-and-distortion ratios (SNDRs) of the HI-HD-SM-MIMO system can be obtained from (13) and (14) by setting the RSI equal to zero, i.e., $\sigma^2_{\mathrm{RSI_A}} = 0$ and $\sigma^2_{\mathrm{RSI_A}} = 0$. Due to the effect of RSI, the performance in terms of OP and SEP of the HI-FD-SM-MIMO system is lower than that of the HI-HI-SM-MIMO system.

It is noted that in the SM-MIMO system, information bits are mapped to not only the transmit symbols but also the indices of the transmission antennas. As a result, the SM-MIMO systems can achieve higher spectral efficiency than the traditional single-input multiple-output (SIMO) systems [5], [15]. Based on the received signals given in (5) and (6), the ML detector jointly detects the activated antenna information and modulated symbols at A and B, i.e.,

$$(\hat{m}, \hat{x}_n) = \arg \min_{(m, x_n)} \|\mathbf{y} - \mathbf{h}_m x_n\|^2, \quad (15)$$

where $m \in \{1, 2, \ldots, N_{\mathrm{t}}\}$, $N_{\mathrm{t}} \in \{N_{\mathrm{tA}}, N_{\mathrm{tB}}\}$, is the index of activated antenna; $x_n \in \{x_i, x_j\}$ is the transmitted symbol.

For realistic SM communication systems, finite alphabet is a more practical input scheme because the index of the transmit antenna used to convey a partial information is discrete and finite. Due to the constraint of finite alphabet inputs, the capacity of the SM system with finite-alphabet input may be lower than that of the SM system with Gaussian inputs. Specifically, when finite-alphabet inputs are used, the ADR (or the mutual information between the input and output variables) is calculated as [40]–[43]

$$\mathcal{R}_{\mathrm{SM}} = I(\mathbf{h}; \mathbf{y}|x) + I(x; \mathbf{y}), \quad (16)$$

where $I(\mathbf{h}; \mathbf{y}|x)$ is the mutual information of the activated antenna information, and $I(x; \mathbf{y})$ is the mutual information between $x$ and $\mathbf{y}$.

Applying [40], [42], [43], the ADR in (16) can be rewritten as in (17), as shown at the bottom of the page, where $\mathbb{E}$ is the expectation operator; $\mathbf{d}_{m,n}^{m_2,n_2} = \mathbf{h}_m x_n - \mathbf{h}_{m_2} x_{n_2}$ with $(m, n) \neq (m_2, n_2)$; $\mathbf{h} \in \{\mathbf{h}_{j\mathrm{A}}, \mathbf{h}_{i\mathrm{B}}\}$; $\eta^{\mathrm{t}} \in \{\eta_j^{\mathrm{t}}, \eta_i^{\mathrm{t}}\}$; $\boldsymbol{\eta}^{\mathrm{r}} \in \{\boldsymbol{\eta}_{\mathrm{A}}^{\mathrm{r}}, \boldsymbol{\eta}_{\mathrm{B}}^{\mathrm{r}}\}$; $\mathbf{r}_{\mathrm{SI}} \in \{\mathbf{r}_{\mathrm{SI_A}}, \mathbf{r}_{\mathrm{SI_B}}\}$; $\mathbf{z} \in \{\mathbf{z}_{\mathrm{A}}, \mathbf{z}_{\mathrm{B}}\}$; $k \in \{k_{\mathrm{A}}, k_{\mathrm{B}}\}$; $P \in \{P_{\mathrm{A}}, P_{\mathrm{B}}\}$; and $\sigma^2 \in \{\sigma^2_{\mathrm{A}}, \sigma^2_{\mathrm{B}}\}$.

With $\mathrm{SNR} = P/\sigma^2$, the maximum ADR in high SNR regime is $\log_2(M_{\mathrm{o}}) + \log_2(N_{\mathrm{t}})$ [40], [42], [43] due to the second term in (17) is very small.

In this paper, the main goal is to analyze the impacts of both HI and RSI as well as the effect of TAS scheme on the performance of FD-SM-MIMO system by mathematically deriving the exact closed-form expressions of OP and SEP. For the sake of simplifying the following analysis of OP, SEP, and ADR similar to [15], [25], [26], [44], we use the upper bound of the ADR, i.e.,

$$\mathcal{R}_{\mathrm{SM}} = \log_2(N_{\mathrm{t}}) + \log_2(M_{\mathrm{o}}), \quad (18)$$

where $N_{\mathrm{t}}$ denotes the number of transmission antennas at terminals A and B, i.e., $N_{\mathrm{t}} \in \{N_{\mathrm{tA}}, N_{\mathrm{tB}}\}$; $M_{\mathrm{o}}$ denotes the modulation constellation size. Note that (18) is the total bits transmitted in an interval, where $\log_2(M_{\mathrm{o}})$ bits is used to selected a symbol $x$ from an M-QAM or M-PSK signal set, while $\log_2(N_{\mathrm{t}})$ bits is used to select an antenna $i$ out of $N_{\mathrm{t}}$ transmit antennas for the transmission of the selected symbol $x$.

## III. PERFORMANCE ANALYSIS

### A. OUTAGE PROBABILITY

The OP of the point-to-point wireless system is defined as follows [45]

$$\mathcal{P} = \Pr\{\log_2(N_{\mathrm{t}}) + \log_2(1 + \gamma) < \mathcal{R}_0\}, \quad (19)$$

where $\gamma$ and $\mathcal{R}_0$ denote the SINDR and transmission rate, respectively. It should be noticed that, the ADR in (19) is the

$$\mathcal{R}_{\mathrm{SM}} = \log_2(M_{\mathrm{o}} N_{\mathrm{t}}) - \frac{1}{M_{\mathrm{o}} N_{\mathrm{t}}} \sum_{m=1}^{N_{\mathrm{t}}} \sum_{n=1}^{M_{\mathrm{o}}} \times \mathbb{E}_{\mathbf{h}\eta^{\mathrm{t}}, \boldsymbol{\eta}^{\mathrm{r}}, \mathbf{r}_{\mathrm{SI}}, \mathbf{z}} \left\{ \log_2 \left[ \sum_{m_2=1}^{N_{\mathrm{t}}} \sum_{n_2=1}^{M_{\mathrm{o}}} \exp\left( - \frac{\|\mathbf{d}_{m,n}^{m_2,n_2} + \mathbf{h}\eta^{\mathrm{t}} + \boldsymbol{\eta}^{\mathrm{r}} + \mathbf{r}_{\mathrm{SI}} + \mathbf{z}\|^2 - \|\mathbf{h}\eta^{\mathrm{t}} + \boldsymbol{\eta}^{\mathrm{r}} + \mathbf{r}_{\mathrm{SI}} + \mathbf{z}\|^2}{k^2 P + \sigma^2_{\mathrm{RSI}} + \sigma^2} \right) \right] \right\} \quad (17)$$

channel capacity, which is the maximum attainable mutual information between the channel input-output of the considered system and expressed as bit per channel use (bpcu).

As given in (13) and (14), the SINDRs at nodes A and B are similar. Thus, the OP and SEP expressions of A and B also have the same form. To simplify the mathematical presentation in this paper, we will provide our analysis for node B in the following parts. The OP and SEP expressions of node A can be obtained in a similar way.

From (19), the OP of B is calculated as

$$\begin{aligned}\mathcal{P}_{\rm B} &= \Pr\{\log_2(N_{\rm tA}) + \log_2(1+\gamma_{\rm B}) < \mathcal{R}_0\} \\ &= \Pr\{\gamma_{\rm B} < 2^{\mathcal{R}_0 - \log_2(N_{\rm tA})} - 1\} \\ &= \Pr\{\gamma_{\rm B} < 2^{\mathcal{R}} - 1\}, \end{aligned} \tag{20}$$

where $\gamma_{\rm B}$ is given in (14); $\mathcal{R} = \mathcal{R}_0 - \log_2(N_{\rm tA})$ denotes the transmission rate obtained by the modulation scheme.

Let $\gamma_{\rm th} = 2^{\mathcal{R}} - 1$ be the threshold, then (20) can be rewritten as

$$\begin{aligned}\mathcal{P}_{\rm B} &= \Pr\left\{\frac{\|\mathbf{h}_{i\rm B}\|^2 \bar{\gamma}_{\rm B}}{\|\mathbf{h}_{i\rm B}\|^2 k_{\rm B}^2 \bar{\gamma}_{\rm B} + 1} < \gamma_{\rm th}\right\} \\ &= \Pr\left\{\|\mathbf{h}_{i\rm B}\|^2 \bar{\gamma}_{\rm B}(1 - k_{\rm B}^2 \gamma_{\rm th}) < \gamma_{\rm th}\right\}. \end{aligned} \tag{21}$$

Based on (21), the OP of the considered HI-FD-SM-MIMO system can be obtained in the following Theorem 1.

*Theorem 1*: When $\gamma_{\rm th} > 1/k_{\rm B}^2$, the OP of terminal B of the considered HI-FD-SM-MIMO system with TAS (denoted by $\mathcal{P}_{\rm B}^{\rm wi}$) is given by (22), as shown at the bottom of the next page, where $B(.,.)$, $\Gamma(.)$ and $\Gamma(.,.)$ are the beta, gamma, and incomplete gamma function [46], respectively; $M$ is the complexity-accuracy trade-off parameter; $\chi_{\rm B} = \frac{\gamma_{\rm th}}{2\bar{\gamma}_{\rm B}(1-k_{\rm B}^2\gamma_{\rm th})}(1+\phi_m)$; $\phi_m = \cos\left(\frac{(2m-1)\pi}{2M}\right)$; $w_{\rm A} = N_{\rm tA} - S_{\rm A} + 1$.

*Proof*: The detailed proof are given in Appendix A.

It is also noted that in the case without TAS, the OP of terminal B (denoted by $\mathcal{P}_{\rm B}^{\rm wo}$) of the considered HI-FD-SM-MIMO system is given by

$$\mathcal{P}_{\rm B}^{\rm wo} = 1 - e^{-\frac{\gamma_{\rm th}}{\bar{\gamma}_{\rm B}(1-k_{\rm B}^2\gamma_{\rm th})}} \sum_{p=0}^{N_{\rm rB}-1} \frac{1}{p!}\left(\frac{\gamma_{\rm th}}{\bar{\gamma}_{\rm B}(1-k_{\rm B}^2\gamma_{\rm th})}\right)^p. \tag{23}$$

Note that, due to the properties of the OP expression, approximating this function in the extreme conditions can cause great errors. Therefore, in this paper, we do not provide asymptotic forms of the OP and the other expressions.

### B. SYMBOL ERROR PROBABILITY

The SEP of the wireless system is computed as [45]

$$\text{SEP} = a\mathbb{E}\{Q(\sqrt{b\gamma})\} = \frac{a}{\sqrt{2\pi}} \int_0^\infty F\left(\frac{t^2}{b}\right) e^{-\frac{t^2}{2}} dt, \tag{24}$$

where $a$ and $b$ are constants whose values depend on the modulation types, e.g., $a = 2, b = 1$ for 4-quadrature amplitude modulation (4-QAM) modulation; $a = 1, b = 2$ for the binary phase-shift keying (BPSK) modulation [45]; $Q(x)$ represents the Gaussian function; $\gamma$ and $F(x)$ are the SINDR and its CDF, respectively. By letting $x = \frac{t^2}{b}$, we can rewrite (24) as

$$\text{SEP} = \frac{a\sqrt{b}}{2\sqrt{2\pi}} \int_0^\infty \frac{e^{-bx/2}}{\sqrt{x}} F(x) dx. \tag{25}$$

Based on (25), we can obtain the SEPs of the considered HI-FD-SM-MIMO system in the following Theorem 2.

*Theorem 2*: The SEP of terminal B of the considered HI-FD-SM-MIMO system with TAS (denoted by $\text{SEP}_{\rm B}^{\rm wi}$) is given by (26), as shown at the bottom of the next page, where $N$ is the complexity-accuracy trade-off parameter; $\phi_n = \cos\left(\frac{(2n-1)\pi}{2N}\right)$. $\psi_{\rm B} = \frac{1+\phi_m}{2\bar{\gamma}_{\rm B}}$; $u = \frac{1}{2k_{\rm B}^2}(1+\phi_n)$.

*Proof*: The detailed proof is provided in Appendix B.

In the case without TAS, the SEP of the terminal B (denoted by $\text{SEP}_{\rm B}^{\rm wo}$) of the HI-FD-SM-MIMO system is given by

$$\begin{aligned}\text{SEP}_{\rm B}^{\rm wo} = \frac{a\sqrt{b}}{2\sqrt{2\pi}}\Bigg[\sqrt{\frac{2\pi}{b}} - \frac{\pi}{2Nk_{\rm B}^2} \sum_{p=0}^{N_{\rm rB}-1}\sum_{n=1}^{N} \frac{u^{p-\frac{1}{2}}}{p!\bar{\gamma}_{\rm B}^p(1-k_{\rm B}^2 u)^p} \\ \times \sqrt{1-\phi_n^2}\, e^{-\frac{u}{(1-k_{\rm B}^2 u)\bar{\gamma}_{\rm B}} - \frac{bu}{2}}\Bigg]. \end{aligned} \tag{27}$$

### C. ACHIEVABLE DATA RATE

The maximum ADR of the considered HI-FD-SM-MIMO system is expressed as

$$\begin{aligned}\mathcal{C} = \log_2(N_{\rm tA}) + \mathbb{E}\Big\{\log_2(1+\gamma_{\rm B})\Big\} \\ + \log_2(N_{\rm tB}) + \mathbb{E}\Big\{\log_2(1+\gamma_{\rm A})\Big\}, \end{aligned} \tag{28}$$

where the terms $\log_2(N_{\rm tA}) + \mathbb{E}\{\log_2(1+\gamma_{\rm B})\}$ and $\log_2(N_{\rm tB}) + \mathbb{E}\{\log_2(1+\gamma_{\rm A})\}$ are the data rates from A to B and from B to A, respectively.

From (28), the maximum ADR of the considered system is derived in the following Theorem 3.

*Theorem 3*: The maximum ADR of the considered HI-FD-SM-MIMO system with TAS (denoted by $\mathcal{C}^{\rm wi}$) is given by (29), as shown at the bottom of the next page, where $N$, $\phi_n$, $\psi_{\rm B}$, and $u$ were defined in Theorem 2.

*Proof*: The detailed proof is provided in Appendix C.

The maximum achievable date rate of the considered HI-FD-SM-MIMO system without TAS (denoted by $\mathcal{C}^{\rm wo}$) is calculated as

$$\begin{aligned}\mathcal{C}^{\rm w0} = 2\log_2(N_{\rm tA}) + \frac{\pi}{Nk_{\rm B}^2 \ln 2} \sum_{p=0}^{N_{\rm rB}-1}\sum_{n=1}^{N} e^{-\frac{u}{(1-k_{\rm B}^2 u)\bar{\gamma}_{\rm B}}} \\ \times \frac{u^p\sqrt{1-\phi_n^2}}{p!(1+u)\bar{\gamma}_{\rm B}^p(1-k_{\rm B}^2 u)^p}. \end{aligned} \tag{30}$$

## IV. NUMERICAL RESULTS AND DISCUSSIONS

In this section, the performance of the considered HI-FD-SM-MIMO system with and without TAS under the impact of RSI is investigated. It is also compared with that

of the ideal-FD-SM-MIMO system to understand about the HI impact. It is noted that the OP expressions of the ideal-FD-SM-MIMO system can be obtained by setting $k_{\rm A} = k_{\rm B} = 0$ in the OP expressions of the HI-FD-SM-MIMO system. Other parameters are set as follows: the average transmission power at two terminals $P_{\rm A} = P_{\rm B} = P$; the variance of the Gaussian noises $\sigma_{\rm A}^2 = \sigma_{\rm B}^2 = \sigma^2 = 1$; the numbers of transmission and reception antennas are $N_{\rm tA} = N_{\rm tB} = N_{\rm t} = 4$ and $N_{\rm rA} = N_{\rm rB} = N_{\rm r} = 2$, respectively; the numbers of the selected transmission antennas are $S_{\rm A} = S_{\rm B} = S = 2$; the HI levels $k_{\rm A}^{\rm t} = k_{\rm A}^{\rm r} = k_{\rm B}^{\rm t} = k_{\rm B}^{\rm r} = k$; the RSI levels $l_{\rm A} = l_{\rm B} = l$. The average SNR is defined as SNR $= P/\sigma^2$. The 4-QAM modulation ($a = 2, b = 1$) is used for all simulations. The simulation results were obtained by using $10^7$ channel realizations. For the sake of simplicity, we will simply use the term "the system performance" instead of mentioning explicitly node A or B in the subsequent discussions. Furthermore, the RSI level, $l$, can be from 0 (perfect SIC) to 1 (without SIC) in practice. However, in the following scenarios, the range of the RSI level is chosen from 0.01 to 0.3, which is based on the recording by measurements and experiments of FD devices [14], [29], [35].

Fig. 2 illustrates the impact of HI on the OPs of the considered HI-FD-SM-MIMO systems in the case with and without TAS for two transmission rates, $\mathcal{R} = 2, 4$ bit-per-channel-use (bpcu). We have used (22) and (23) to plot the OPs of the HI-FD-SM-MIMO systems in the case with and without TAS, respectively. We have also replaced $k = 0$ in (22) and (23) to obtain the OP curves of the ideal-FD-SM-MIMO systems with and without TAS. It can be seen in Fig. 2 that for low data transmission rate, i.e., $\mathcal{R} = 2$ bpcu, the OPs

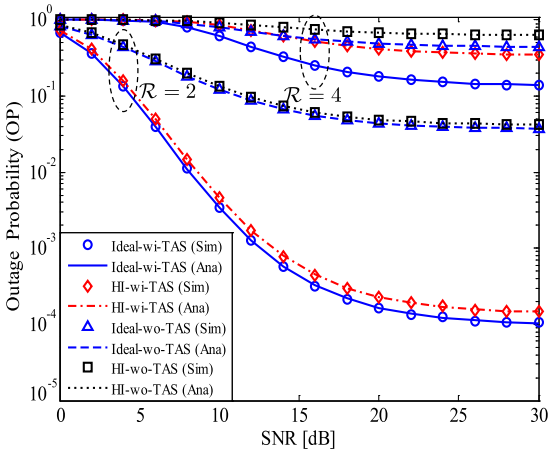


**FIGURE 2. The impact of HI on the OPs of the considered HI-FD-SM-MIMO systems with and without TAS versus the average SNR for different data transmission rates; $N_{\rm t} = 4$, $S = 2$, $N_{\rm r} = 2$, $l = -5$ dB, $k = 0.1$.**

of both the FD-SM-MIMO system with and without HI are similar. This means the performance degradation due to HI is negligibly small for this system. However, in the case of higher transmission rate, i.e., $\mathcal{R} = 4$ bpcu, the impact of HI becomes larger and cannot be neglected. It can also be seen that TAS significantly reduces the OPs of both the system with and without HI. With the given parameters, the OPs for the case without TAS reach $6 \times 10^{-2}$ while those with TAS reach $2 \times 10^{-4}$ for both the systems at high SNR regime for $\mathcal{R} = 2$ bpcu. This leads to the conclusion that TAS can greatly improve the OP performance of the FD-SM-MIMO system under the joint impact of both HI and RSI.

$$\mathcal{P}_{\rm B}^{\rm wi} = \frac{\pi\gamma_{\rm th}}{2M(N_{\rm tA}-w_{\rm A}+1)\Gamma(N_{\rm rB})\bar{\gamma}_{\rm B}(1-k_{\rm B}^2\gamma_{\rm th})}\sum_{p=w_{\rm A}}^{N_{\rm tA}}\sum_{m=1}^{M}\frac{\sqrt{1-\phi_m^2}}{B(p,N_{\rm tA}-p+1)} \times\left(1-\frac{\Gamma(N_{\rm rB},\chi_{\rm B})}{\Gamma(N_{\rm rB})}\right)^{p-1}\left(\frac{\Gamma(N_{\rm rB},\chi_{\rm B})}{\Gamma(N_{\rm rB})}\right)^{N_{\rm tA}-p}\chi_{\rm B}^{N_{\rm rB}-1}e^{-\chi_{\rm B}}, \tag{22}$$

$$\mathrm{SEP}_{\rm B}^{\rm wi} = \frac{a\sqrt{b}}{2\sqrt{2\pi}}\Bigg[\frac{\pi^2}{4MNk_{\rm B}^2(N_{\rm tA}-w_{\rm A}+1)\Gamma(N_{\rm rB})\bar{\gamma}_{\rm B}}\sum_{p=w_{\rm A}}^{N_{\rm tA}}\sum_{m=1}^{M}\sum_{n=1}^{N}\frac{\psi_{\rm B}^{N_{\rm rB}-1}\sqrt{(1-\phi_m^2)(1-\phi_n^2)}}{B(p,N_{\rm tA}-p+1)}\left(1-\frac{\Gamma(N_{\rm rB},\frac{\psi_{\rm B}u}{1-k_{\rm B}^2u})}{\Gamma(N_{\rm rB})}\right)^{p-1} \times\left(\frac{\Gamma(N_{\rm rB},\frac{\psi_{\rm B}u}{1-k_{\rm B}^2u})}{\Gamma(N_{\rm rB})}\right)^{N_{\rm tA}-p}\frac{u^{N_{\rm rB}-\frac{1}{2}}}{(1-k_{\rm B}^2u)^{N_{\rm rB}}}e^{-\frac{\psi_{\rm B}u}{1-k_{\rm B}^2u}-\frac{bu}{2}}+\sqrt{\frac{2\pi}{b}}\left(1-\mathrm{erf}\left(\sqrt{\frac{b}{2k_{\rm B}^2}}\right)\right)\Bigg] \tag{26}$$

$$\mathcal{C}^{\rm wi} = 2\log_2(N_{\rm tA})+2\log_2\frac{1+k_{\rm B}^2}{k_{\rm B}^2}-\frac{\pi^2}{2MNk_{\rm B}^2(N_{\rm tA}-w_{\rm A}+1)\Gamma(N_{\rm rB})\bar{\gamma}_{\rm B}\ln 2}\sum_{p=w_{\rm A}}^{N_{\rm tA}}\sum_{m=1}^{M}\sum_{n=1}^{N}\frac{\psi_{\rm B}^{N_{\rm rB}-1}\sqrt{(1-\phi_m^2)(1-\phi_n^2)}}{B(p,N_{\rm tA}-p+1)} \times\left(1-\frac{\Gamma(N_{\rm rB},\frac{\psi_{\rm B}u}{1-k_{\rm B}^2u})}{\Gamma(N_{\rm rB})}\right)^{p-1}\left(\frac{\Gamma(N_{\rm rB},\frac{\psi_{\rm B}u}{1-k_{\rm B}^2u})}{\Gamma(N_{\rm rB})}\right)^{N_{\rm tA}-p}\frac{u^{N_{\rm rB}}}{(1-k_{\rm B}^2u)^{N_{\rm rB}}(1+u)}e^{-\frac{\psi_{\rm B}u}{1-k_{\rm B}^2u}} \tag{29}$$

To clearly show the benefit of TAS, in Fig. 3, we consider the case of larger numbers of transmission antennas and selected antennas, i.e., $N_t = 8$ and $S = 4$. This parameter configuration results in $\mathcal{R}_0$ with 1 bpcu higher than the previous case. As observed from Fig. 3, TAS is really effective for mitigating the impact of HI, especially for the case of low transmission rate ($\mathcal{R} = 2$ bpcu). It is because the system with more transmission antennas has higher diversity gain, which then helps to lower the outage floor. However, when the system with higher transmission rate ($\mathcal{R} = 4$ bpcu) is more affected by HI, the advantage of TAS on its OP performance is not significant. It is also noted that, when the numbers of transmission antennas increases, the total data rate ($\mathcal{R}_0$) increases and may be different for the cases with and without TAS. However, the data rate due to modulation scheme ($\mathcal{R}$) is still similar for these cases.

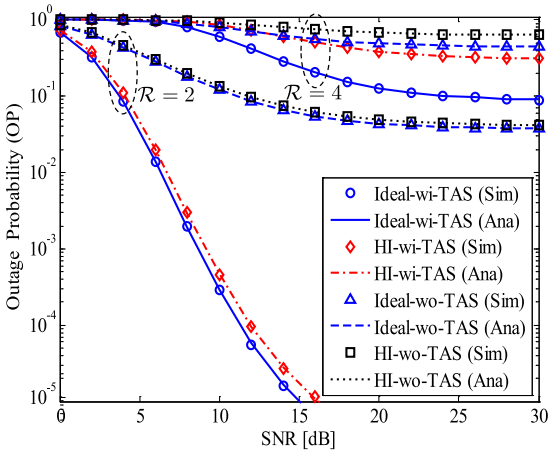


**FIGURE 3.** The impact of HI on the OPs of the considered HI-FD-SM-MIMO systems with and without TAS versus the average SNR for different data transmission rates; $N_t = 8$, $S = 4$, $N_r = 2$, $l = -5$ dB, $k = 0.1$.

Fig. 4 investigates the throughput $\mathcal{T}$ of the considered HI-FD-SM-MIMO system. It is calculated as $\mathcal{T} = \mathcal{R}(1 - \mathcal{P})$ where $\mathcal{P}$ is given in (22) for the case with TAS and in (23) for the case without TAS. The throughputs of the ideal-FD-SM-MIMO system with and without TAS are obtained similarly as for the OPs. For low data transmission rate, i.e., $\mathcal{R} = 2$ bpcu, both the systems with TAS reach the target throughput of 2 bpcu at SNR $= 8$ dB. However, in the case without TAS, the throughput of both the systems only reach 1.9 bpcu at SNR $= 16$ dB. Particularly, for high transmission rate, i.e., $\mathcal{R} = 4$ bpcu, none of the systems with TAS can reach the target throughput of 4 bpcu. This is due to the strong impact of RSI on the system throughput. Meanwhile, the considered HI-FD-SM-MIMO system can only reach the throughput of 2.6 bpcu due to the joint impact of both HI and RSI. For the case without TAS, both the systems can reach the throughput of 1.5 and 2.2 bpcu, respectively. From both Fig. 2 and Fig. 4 we can see that the HI-FD-SM-MIMO system with high transmission rate is greatly influenced by HI. Therefore, when HI exists, the usage of a low data transmission rate is necessary to reduce the performance and throughput losses. In such a case, TAS can be used as an effective solution to improve the system performance.

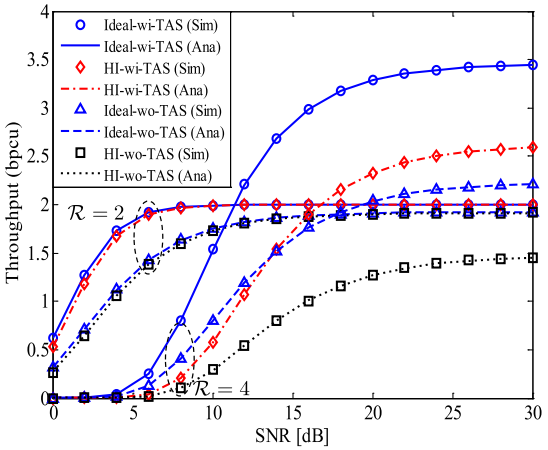


**FIGURE 4.** The throughput of the considered HI-FD-SM-MIMO system in comparison with that of ideal-FD-SM-MIMO system in the cases with and without TAS, $l = -5$ dB, $k = 0.1$, $\mathcal{R} = 2, 4$ bpcu.

Fig. 5 plots the SEPs of the considered HI-FD-SM-MIMO systems in the case with and without TAS versus the average SNR. The RSI and HI levels are respectively set as $l_A = l_B = -5$ dB and $k = 0.15$. We use (26) and (27) to obtain the analytical results of the HI-FD-SM-MIMO systems with and without TAS, respectively. The simulated SEPs of the ideal-FD-SM-MIMO systems with and without TAS are provided for comparison. Additionally, we also provide the SEPs of the HI-FD-SM-MIMO systems in the case of imperfect detection the activated antenna indices with and without TAS, denoted by "HI-wi-TAS-I" and "HI-wi-TAS-I", respectively. It is noted that we can obtain the OP expressions of the ideal-FD-SM-MIMO systems from the OP expressions of the HI-FD-SM-MIMO systems by replacing $k_A = k_B = 0$ in (22)

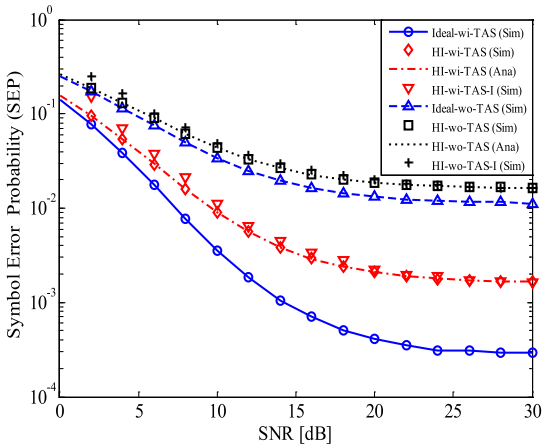


**FIGURE 5.** The SEPs of the considered HI-FD-SM-MIMO systems with and without TAS versus the average SNR for $N_t = 4$, $S = 2$, $N_r = 2$, $l = -5$ dB, $k = 0.15$.

and (23). However, we cannot obtain the SEP expressions of the ideal-FD-SM-MIMO systems from the SEP expressions of the HI-FD-SM-MIMO systems by a similar approach due to th existence of the terms $1/k_{\mathrm{A}}^2$ and $1/k_{\mathrm{B}}^2$ in (26) and (27). As can be seen from Fig. 5 that all SEP curves have an error floor in the high SNR regime (SNR = 30 dB). Furthermore, the performance degradation due to HI in the case without TAS is smaller than the case with TAS. Specifically, for the case with TAS, the error floor of the considered system is $1.7 \times 10^{-3}$ while it is $2.9 \times 10^{-4}$ for the ideal system. For the case without TAS, it is nearly $1.7 \times 10^{-2}$ for both the systems. These results clearly demonstrate the benefits of using TAS for the FD-SM-MIMO system. On the other hand, the index antenna detection errors are high in low SNR regime, however, there is no index antenna detection error in high SNR regime for the considered HI-FD-SM-MIMO systems with and without TAS. That validates our mathematical expressions in the paper.

Fig. 6 depicts the joint impact of HI and RSI on the SEPs. From this figure we can easily deduce the SEPs of other related systems, such as ideal-FD-SM-MIMO, ideal-HD-SM-MIMO, HI-HD-SM-MIMO systems. For example, for ($k \approx 0$, $l \approx 0$), ($k > 0$, $l \approx 0$) and ($k \approx 0$, $l > 0$) the SEPs of the HI-FD-SM-MIMO become those of the ideal-HD-SM-MIMO, HI-HD-SM-MIMO and ideal-FD-SM-MIMO systems, respectively. As can be seen from Fig. 6, SEP increases rapidly with both $k$ and $l$, especially in the high value regime. Particularly, we have SEP $= 7.5 \times 10^{-5}$ and SEP $= 2.4 \times 10^{-3}$ when $k = 0.15$ and $l = 0.15$ while SEP $= 10^{-8}$ and SEP $= 2.4 \times 10^{-4}$ when $k \approx 0$ and $l \approx 0$ (the ideal-HD-SM-MIMO system) for the cases with and without TAS, respectively. In other words, both $k$ and $l$ cause great performance degradation in the considered HI-FD-SM-MIMO system.

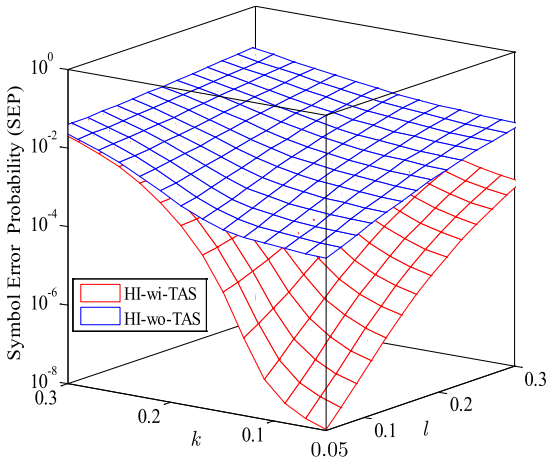


**FIGURE 6.** The joint impact of both HI and RSI on the SEPs of the considered HI-FD-SM-MIMO systems with and without TAS, SNR = 20 dB.

Fig. 7 shows the maximum ADRs of the considered HI-FD-SM-MIMO systems with and without TAS versus the average SNR for $N_{\mathrm{t}} = 4$, $S = 2$, $N_{\mathrm{r}} = 2$, $l = -5$ dB,

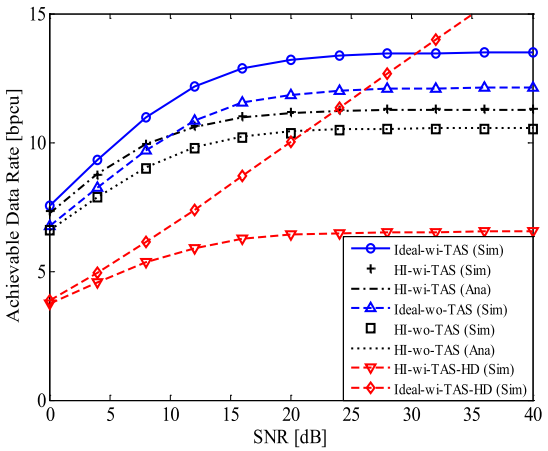


**FIGURE 7.** The maximum ADRs of the considered HI-FD-SM-MIMO systems with and without TAS versus the average SNR for $N_{\mathrm{t}} = 4$, $S = 2$, $N_{\mathrm{r}} = 2$, $l = -5$ dB, $k = 0.15$.

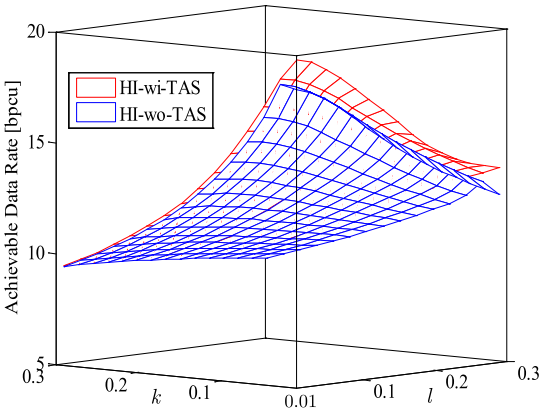


**FIGURE 8.** The maximum ADRs of the considered HI-FD-SM-MIMO systems with and without TAS under the joint impact of the HI and RSI for $N_{\mathrm{t}} = 4$, $S = 2$, $N_{\mathrm{r}} = 2$.

$k = 0.15$. The analytical results with and without TAS are plotted using (29) and (30), respectively, to demonstrate the benefits of the FD technique and the impact of the RSI on the HI-FD-SM-MIMO system's ADR. In addition, the ADR of the Ideal-HD-SM-MIMO system with TAS is also given for easy comparison. It is obvious from Fig. 7 that, the impact of the HI on the ADR is stronger than that on the SEP because the SEP performance in the case of HI with TAS is higher than that in the case of the ideal without TAS (refer to Fig. 5) while the ADR in the case of HI with TAS is lower than that in the case of the ideal without TAS (refer to Fig. 7). Particularly, at SNR = 30 dB, the ADRs with TAS are only 1.2 bpcu higher than the case of without TAS and 0.8 bpcu higher than the cases of ideal and HI. By combining Fig. 5 and Fig. 7, we can conclude that applying TAS for the considered HI-FD-SM-MIMO systems significantly decreases the SEP but slightly increases the ADRs compared to the case without TAS. Furthermore, with investigated parameters, the HI-FD-SM-MIMO system's ADR is always higher than that of the HI-HD-SM-MIMO system. However, for the ideal hardware

systems, the ADR of the Ideal-FD-SM-MIMO system is only higher than that of the Ideal-HD-SM-MIMO system when SNR $<$ 30 dB. As SNR $>$ 30 dB, the ADR of the Ideal-FD-SM-MIMO system is lower than that of Ideal-HD-SM-MIMO system. This feature emphasizes the strong influence of the RSI on the performance of the considered HI-FD-SM-MIMO system in the high SNR regime.

Fig. 8 illustrates the HI and RSI's joint impact on the maximum ADRs of the considered HI-FD-SM-MIMO systems with and without TAS. Similar to Fig. 7, the benefits of using TAS on the ADR are not significant. On the other hand, when both $k$ and $l$ change from 0.01 to 0.3, the difference between the ADRs with and without TAS remains unchanged. This is the major difference between SEP and the ADR. In particular, the SEPs with and without TAS are $10^{-8}$ and $10^{-4}$, respectively, when $k = l = 0.05$ (refer to Fig. 6). Meanwhile, the ADRs with and without TAS are 17.2 and 16.6 bpcu, respectively, when $k = l = 0.05$ (refer to Fig. 8). Another observation is that all SEP curves (Fig. 5 and Fig. 6) exhibit irreducible error floors and all ADR curves (Fig. 7 and Fig. 8) exhibit irreducible rate floors due to HI distortion and RSI. Furthermore, the variances of both HI distortion and RSI are the functions of transmission power. Therefore, increasing SNR helps to reduce SEP and increase the ADR. When the SNR is small, the levels of HI distortion and RSI are similar to noise levels. However, when SNR is larger, the levels of HI and RSI become dominant. Thus, the SEP and the ADR are saturated quickly, causing irreducible floors of SEP and the ADR. It is worth noticing that, since TAS is used not for mitigating HI and RSI but for obtaining the spatial diversity, this solution can only decrease SEP and increase the ADR but cannot eliminate their floors.

## V. CONCLUSION

Hardware impairments are important factors that need to be considered when establishing wireless networks, especially for the high rate systems. In this paper, we considered the FD-SM-MIMO system under the joint impact of HI and RSI. In order to compensate the performance degradation due to these factors, we proposed to use TAS in this system. Using theoretical analysis we obtained the closed-form expressions of the OP, throughput, SEP, and ADR in the case of perfect antenna index estimation. It was first seen that besides degradation, HI and RSI also cause these performance parameters to saturate in the high SNR regime. Moreover, it was also understood that HI has a stronger impact than RSI does. The proposed TAS solution was shown to be a simple yet effective solution for performance improvement. However, in order to tackle fully the impacts of HI and RSI, more effective methods to suppress these distortions still need to be further studied.

## APPENDIX A

This appendix provides the detailed derivation of the OP of the HI-FD-SM-MIMO system using TAS.

In order to obtain the OP expression from (21), we need to consider the following two cases: $1 - k_{\mathrm{B}}^2\gamma_{\mathrm{th}} \leq 0$ and $1 - k_{\mathrm{B}}^2\gamma_{\mathrm{th}} > 0$.

Case 1: $1-k_{\mathrm{B}}^2\gamma_{\mathrm{th}} \leq 0$ or $\gamma_{\mathrm{th}} \geq 1/k_{\mathrm{B}}^2$. The probability in (21) is always true, due to the fact that $\|\mathbf{h}_{i\mathrm{B}}\|^2\bar{\gamma}_{\mathrm{B}}(1 - k_{\mathrm{B}}^2\gamma_{\mathrm{th}}) \leq 0$ while $\gamma_{\mathrm{th}} > 0$. Therefore, $\mathcal{P}_{\mathrm{B}} = 1$ for both the cases with and without TAS.

Case 2: $1 - k_{\mathrm{B}}^2\gamma_{\mathrm{th}} > 0$ or $\gamma_{\mathrm{th}} < 1/k_{\mathrm{B}}^2$. The probability in (21) can be rewritten as

$$\begin{aligned}\mathcal{P}_{\mathrm{B}} &= \Pr\left\{\|\mathbf{h}_{i\mathrm{B}}\|^2\bar{\gamma}_{\mathrm{B}}(1 - k_{\mathrm{B}}^2\gamma_{\mathrm{th}}) < \gamma_{\mathrm{th}}\right\} \\ &= \Pr\left\{\|\mathbf{h}_{i\mathrm{B}}\|^2 < \frac{\gamma_{\mathrm{th}}}{\bar{\gamma}_{\mathrm{B}}(1 - k_{\mathrm{B}}^2\gamma_{\mathrm{th}})}\right\}. \end{aligned} \tag{31}$$

Using (31), the OP expression in Theorem 1 is determined through the following steps.

First, the probability density function (PDF, denoted by $f(x)$) and the cumulative distribution function (CDF, denoted by $F(x)$) of the random instantaneous channel gain $|h|^2$ of the Rayleigh fading channel are, respectively, given by

$$f_{|h|^2}(x) = \frac{1}{\Omega}e^{-\frac{x}{\Omega}}, \quad x \geqslant 0, \tag{32}$$

$$F_{|h|^2}(x) = \Pr\{|h|^2 < x\} = 1 - e^{-\frac{x}{\Omega}}, \quad x \geqslant 0, \tag{33}$$

where $\Omega = \mathbb{E}\{|h|^2\}$ denotes the average channel gain. In this paper, we normalize the average channel gain, i.e., $\Omega = 1$, for all channels.

When the MRC technique is applied at the receiver, we have the sum of $N_{\mathrm{r}}$ channel gains $Y = \|\mathbf{h}_{i\mathrm{B}}\|^2 = \sum_{l=1}^{N_{\mathrm{rB}}} |h_{il}|^2$. In this case, the PDF and CDF of $Y$ are respectively expressed as

$$f_Y(x) = \frac{x^{N_{\mathrm{rB}}-1}e^{-x}}{\Gamma(N_{\mathrm{rB}})}, \quad x \geq 0. \tag{34}$$

$$F_Y(x) = 1 - e^{-x}\sum_{p=0}^{N_{\mathrm{rB}}-1}\frac{x^p}{p!}, \quad x \geq 0. \tag{35}$$

In contrast, when TAS scheme is used, the sums of the channel gains will be rearranged in a descending order. From this new set, $S$ antennas ($S_{\mathrm{A}}$ of terminal A and $S_{\mathrm{B}}$ of terminal B) will be selected to maximize the received power. For terminal B, the PDF of $Y_{w_{\mathrm{A}}\mathrm{B}}$ in the case that $Y_{1\mathrm{B}} \leq Y_{2\mathrm{B}} \leq \ldots \leq Y_{w_{\mathrm{A}}\mathrm{B}} \leq \ldots \leq Y_{N_{\mathrm{tA}}\mathrm{B}}$ is computed as [47, Eq. 2.1.6]

$$\begin{aligned} f_{Y_{w_{\mathrm{A}}\mathrm{B}}}(x) = &\frac{1}{B(w_{\mathrm{A}}, N_{\mathrm{tA}} - w_{\mathrm{A}} + 1)} \\ &\times \Big(F_Y(x)\Big)^{w_{\mathrm{A}}-1}\Big(1 - F_Y(x)\Big)^{N_{\mathrm{tA}}-w_{\mathrm{A}}} f_Y(x). \end{aligned} \tag{36}$$

Therefore, the PDF of the instantaneous $\|\mathbf{h}_{i\mathrm{B}}\|^2$ in the case with TAS is then given by [26]

$$\begin{aligned} f_{\|\mathbf{h}_{i\mathrm{B}}\|^2}(x) = &\frac{1}{N_{\mathrm{tA}} - w_{\mathrm{A}} + 1}\sum_{p=w_{\mathrm{A}}}^{N_{\mathrm{tA}}}\frac{1}{B(p, N_{\mathrm{tA}} - p + 1)} \\ &\times \Big(F_Y(x)\Big)^{p-1}\Big(1 - F_Y(x)\Big)^{N_{\mathrm{tA}}-p} f_Y(x). \end{aligned} \tag{37}$$

Plugging $F_Y(x)$ and $f_Y(x)$ in (35) and (34) into (37), we obtain the PDF of the instantaneous $\|\mathbf{h}_{iB}\|^2$ as (38), as shown at the bottom of the page.

Since the finite sum in (38) can be calculated as [46]

$$\sum_{p=0}^{N_{\rm rB}-1}\frac{x^p}{p!}=e^x\frac{\Gamma(N_{\rm rB},x)}{\Gamma(N_{\rm rB})},$$

we can rewrite (38) as (39).

From (31) and (39), as shown at the bottom of the page, we obtain the OP for B in the case with TAS as (40), as shown at the bottom of the page. Now applying the Gaussian-Chebyshev quadrature method [48], the integral in (40) is calculated as (41), as shown at the bottom of the page.

Finally, replacing (41) into (40), we obtain the OP expression of terminal B as in (22) of Theorem 1. The OP expression of terminal A is obtained by a similar way. The proof is thus complete.

## APPENDIX B

This appendix provides the detailed derivation of the SEPs of the considered HI-FD-SM-MIMO system.

In order to obtain the $\text{SEP}_{\rm B}$, we first obtain the CDF of the SINDR at terminal B of the considered system. The CDF of the SINDR [45] at terminal B is given by

$$F_{\gamma_{\rm B}}(x)=\Pr\{\gamma_{\rm B}<x\}. \tag{42}$$

Comparing (20) with (42), we can obtain the CDF of the SINDR at terminal B via the OP expression which is calculated in (22) by replacing $\gamma_{\rm th}$ with $x$. The term $\chi_{\rm B}$ then becomes $\chi_{\rm B}=\frac{x(1+\phi_m)}{2\bar{\gamma}_{\rm B}(1-k_{\rm B}^2x)}=\frac{\psi_{\rm B}x}{1-k_{\rm B}^2x}$, where $\psi_{\rm B}=\frac{1+\phi_m}{2\bar{\gamma}_{\rm B}}$. Therefore, $F_{\gamma_{\rm B}}(x)$ is given by (43), as shown at the bottom of the page.

As $F_{\gamma_{\rm B}}(x)$ can be calculated in a similar way with the OP of terminal B. Therefore, $F_{\gamma_{\rm B}}(x)$ is computed as in (43) when $x<1/k_{\rm B}^2$. Otherwise, we have $F_{\gamma_{\rm B}}(x)=1$.

From (25), we have the $\text{SEP}_{\rm B}$ in the case of TAS as (44), as shown at the bottom of the next page. The expression in (44) is rewritten as (45), as shown at the bottom of the next page.

The first integral in (45) can be solved by applying the Gaussian-Chebyshev quadrature method [48] presented in (46), as shown at the bottom of the next page, where $N$ and $u$ are defined as in Theorem 2.

$$f_{\|\mathbf{h}_{iB}\|^2}(x)=\frac{1}{N_{\rm tA}-w_{\rm A}+1}\sum_{p=w_{\rm A}}^{N_{\rm tA}}\frac{1}{B(p,N_{\rm tA}-p+1)}\left(1-e^{-x}\sum_{p=0}^{N_{\rm rB}-1}\frac{x^p}{p!}\right)^{p-1}\left(e^{-x}\sum_{p=0}^{N_{\rm rB}-1}\frac{x^p}{p!}\right)^{N_{\rm tA}-p}\frac{x^{N_{\rm rB}-1}e^{-x}}{\Gamma(N_{\rm rB})}. \tag{38}$$

$$f_{\|\mathbf{h}_{iB}\|^2}(x)=\frac{1}{N_{\rm tA}-w_{\rm A}+1}\sum_{p=w_{\rm A}}^{N_{\rm tA}}\frac{1}{B(p,N_{\rm tA}-p+1)}\left(1-\frac{\Gamma(N_{\rm rB},x)}{\Gamma(N_{\rm rB})}\right)^{p-1}\left(\frac{\Gamma(N_{\rm rB},x)}{\Gamma(N_{\rm rB})}\right)^{N_{\rm tA}-p}\frac{x^{N_{\rm rB}-1}e^{-x}}{\Gamma(N_{\rm rB})}. \tag{39}$$

$$\begin{aligned}\mathcal{P}_{\rm B}^{\rm wi}&=\Pr\left\{\|\mathbf{h}_{iB}\|^2<\frac{\gamma_{\rm th}}{\bar{\gamma}_{\rm B}(1-k_{\rm B}^2\gamma_{\rm th})}\right\}=\int_0^{\frac{\gamma_{\rm th}}{\bar{\gamma}_{\rm B}(1-k_{\rm B}^2\gamma_{\rm th})}}f_{\|\mathbf{h}_{iB}\|^2}(x)dx\\&=\frac{1}{(N_{\rm tA}-w_{\rm A}+1)\Gamma(N_{\rm rB})}\sum_{p=w_{\rm A}}^{N_{\rm tA}}\frac{1}{B(p,N_{\rm tA}-p+1)}\int_0^{\frac{\gamma_{\rm th}}{\bar{\gamma}_{\rm B}(1-k_{\rm B}^2\gamma_{\rm th})}}\left(1-\frac{\Gamma(N_{\rm rB},x)}{\Gamma(N_{\rm rB})}\right)^{p-1}\left(\frac{\Gamma(N_{\rm rB},x)}{\Gamma(N_{\rm rB})}\right)^{N_{\rm tA}-p}x^{N_{\rm rB}-1}e^{-x}dx.\end{aligned} \tag{40}$$

$$\begin{aligned}&\int_0^{\frac{\gamma_{\rm th}}{\bar{\gamma}_{\rm B}(1-k_{\rm B}^2\gamma_{\rm th})}}\left(1-\frac{\Gamma(N_{\rm rB},x)}{\Gamma(N_{\rm rB})}\right)^{p-1}\left(\frac{\Gamma(N_{\rm rB},x)}{\Gamma(N_{\rm rB})}\right)^{N_{\rm tA}-p}x^{N_{\rm rB}-1}e^{-x}dx\\&=\frac{\pi\gamma_{\rm th}}{2M\bar{\gamma}_{\rm B}(1-k_{\rm B}^2\gamma_{\rm th})}\sum_{m=1}^{M}\sqrt{1-\phi_m^2}\left[1-\frac{\Gamma(N_{\rm rB},\chi_{\rm B})}{\Gamma(N_{\rm rB})}\right]^{p-1}\left[\frac{\Gamma(N_{\rm rB},\chi_{\rm B})}{\Gamma(N_{\rm rB})}\right]^{N_{\rm tA}-p}\chi_{\rm B}^{N_{\rm rB}-1}e^{-\chi_{\rm B}}.\end{aligned} \tag{41}$$

$$\begin{aligned}F_{\gamma_{\rm B}}(x)=&\frac{\pi x}{2M(N_{\rm tA}-w_{\rm A}+1)\Gamma(N_{\rm rB})\bar{\gamma}_{\rm B}(1-k_{\rm B}^2x)}\sum_{p=w_{\rm A}}^{N_{\rm tA}}\sum_{m=1}^{M}\frac{\sqrt{1-\phi_m^2}}{B(p,N_{\rm tA}-p+1)}\\&\times\left(1-\frac{\Gamma(N_{\rm rB},\frac{\psi_{\rm B}x}{1-k_{\rm B}^2x})}{\Gamma(N_{\rm rB})}\right)^{p-1}\left(\frac{\Gamma(N_{\rm rB},\frac{\psi_{\rm B}x}{1-k_{\rm B}^2x})}{\Gamma(N_{\rm rB})}\right)^{N_{\rm tA}-p}\left(\frac{\psi_{\rm B}x}{1-k_{\rm B}^2x}\right)^{N_{\rm rB}-1}e^{-\frac{\psi_{\rm B}x}{1-k_{\rm B}^2x}}.\end{aligned} \tag{43}$$

To solve the second integral in (45), we apply [46, Eq. 3.361.1 and Eq. 3.361.2], i.e.,

$$\int_{1/k_{\rm B}^2}^{\infty} \frac{e^{-\frac{bx}{2}}}{\sqrt{x}}dx = \int_{0}^{\infty} \frac{e^{-\frac{bx}{2}}}{\sqrt{x}}dx - \int_{0}^{1/k_{\rm B}^2} \frac{e^{-\frac{bx}{2}}}{\sqrt{x}}dx = \sqrt{\frac{2\pi}{b}}\left(1-\text{erf}\left(\sqrt{\frac{b}{2k_{\rm B}^2}}\right)\right). \quad (47)$$

Substituting (46) and (47) into (45), we obtain the $\text{SEP}_{\rm B}$ as given in (26) of Theorem 2. Using the similar method, we can obtain the $\text{SEP}_{\rm A}$ of the considered system. The proof is thus complete.

## APPENDIX C

This appendix provides the detailed derivation of the maximum ADR of the considered HI-FD-SM-MIMO system.

From (28), we have

$$\mathcal{C} = \log_2(N_{\rm tA}) + \log_2(N_{\rm tB}) + \int_0^{\infty} \log_2(1+\gamma_{\rm A}) f_{\gamma_{\rm A}}(x)dx + \int_0^{\infty} \log_2(1+\gamma_{\rm B}) f_{\gamma_{\rm B}}(x)dx. \quad (48)$$

$$\text{SEP}_{\rm B}^{\rm wi} = \frac{a\sqrt{b}}{2\sqrt{2\pi}}\Bigg[\int_0^{1/k_{\rm B}^2} \frac{e^{-bx/2}}{\sqrt{x}} \frac{\pi x}{2M(N_{\rm tA}-w_{\rm A}+1)\Gamma(N_{\rm rB})\bar{\gamma}_{\rm B}(1-k_{\rm B}^2x)} \sum_{p=w_{\rm A}}^{N_{\rm tA}}\sum_{m=1}^{M} \frac{\sqrt{1-\phi_m^2}}{B(p,N_{\rm tA}-p+1)} \times \left(1-\frac{\Gamma(N_{\rm rB},\frac{\psi_{\rm B}x}{1-k_{\rm B}^2x})}{\Gamma(N_{\rm rB})}\right)^{p-1} \left(\frac{\Gamma(N_{\rm rB},\frac{\psi_{\rm B}x}{1-k_{\rm B}^2x})}{\Gamma(N_{\rm rB})}\right)^{N_{\rm tA}-p} \left(\frac{\psi_{\rm B}x}{1-k_{\rm B}^2x}\right)^{N_{\rm rB}-1} e^{-\frac{\psi_{\rm B}x}{1-k_{\rm B}^2x}}dx + \int_{1/k_{\rm B}^2}^{\infty} \frac{e^{-bx/2}}{\sqrt{x}}dx\Bigg]. \quad (44)$$

$$\text{SEP}_{\rm B}^{\rm wi} = \frac{a\sqrt{b}}{2\sqrt{2\pi}}\Bigg[\frac{\pi\psi_{\rm B}^{N_{\rm rB}-1}}{2M(N_{\rm tA}-w_{\rm A}+1)\Gamma(N_{\rm rB})\bar{\gamma}_{\rm B}} \sum_{p=w_{\rm A}}^{N_{\rm tA}}\sum_{m=1}^{M} \frac{\sqrt{1-\phi_m^2}}{B(p,N_{\rm tA}-p+1)} \int_0^{1/k_{\rm B}^2} \left(1-\frac{\Gamma(N_{\rm rB},\frac{\psi_{\rm B}x}{1-k_{\rm B}^2x})}{\Gamma(N_{\rm rB})}\right)^{p-1} \times \left(\frac{\Gamma(N_{\rm rB},\frac{\psi_{\rm B}x}{1-k_{\rm B}^2x})}{\Gamma(N_{\rm rB})}\right)^{N_{\rm tA}-p} \frac{x^{N_{\rm rB}-\frac{1}{2}}}{(1-k_{\rm B}^2x)^{N_{\rm rB}}} e^{-\frac{\psi_{\rm B}x}{1-k_{\rm B}^2x}-\frac{bx}{2}}dx + \int_{1/k_{\rm B}^2}^{\infty} \frac{e^{-\frac{bx}{2}}}{\sqrt{x}}dx\Bigg]. \quad (45)$$

$$\int_0^{1/k_{\rm B}^2} \left(1-\frac{\Gamma(N_{\rm rB},\frac{\psi_{\rm B}x}{1-k_{\rm B}^2x})}{\Gamma(N_{\rm rB})}\right)^{p-1} \left(\frac{\Gamma(N_{\rm rB},\frac{\psi_{\rm B}x}{1-k_{\rm B}^2x})}{\Gamma(N_{\rm rB})}\right)^{N_{\rm tA}-p} \frac{x^{N_{\rm rB}-\frac{1}{2}}}{(1-k_{\rm B}^2x)^{N_{\rm rB}}} e^{-\frac{\psi_{\rm B}x}{1-k_{\rm B}^2x}-\frac{bx}{2}}dx = \frac{\pi}{2Nk_{\rm B}^2}\sum_{n=1}^{N}\sqrt{1-\phi_n^2}\left(1-\frac{\Gamma(N_{\rm rB},\frac{\psi_{\rm B}u}{1-k_{\rm B}^2u})}{\Gamma(N_{\rm rB})}\right)^{p-1} \left(\frac{\Gamma(N_{\rm rB},\frac{\psi_{\rm B}u}{1-k_{\rm B}^2u})}{\Gamma(N_{\rm rB})}\right)^{N_{\rm tA}-p} \frac{u^{N_{\rm rB}-\frac{1}{2}}}{(1-k_{\rm B}^2u)^{N_{\rm rB}}} e^{-\frac{\psi_{\rm B}u}{1-k_{\rm B}^2u}-\frac{bu}{2}}, \quad (46)$$

$$\mathcal{C}^{\rm wi} = 2\log_2(N_{\rm tA}) + \frac{2}{\ln 2}\int_0^{\infty}\frac{1-F_{\rm B}(x)}{1+x}dx = 2\log_2(N_{\rm tA}) + \frac{2}{\ln 2}\int_0^{\frac{1}{k_{\rm B}^2}}\frac{1-F_{\rm B}(x)}{1+x}dx + \frac{2}{\ln 2}\int_{\frac{1}{k_{\rm B}^2}}^{\infty}\frac{1-F_{\rm B}(x)}{1+x}dx. \quad (50)$$

$$\int_0^{\frac{1}{k_{\rm B}^2}}\frac{1-F_{\rm B}(x)}{1+x}dx = \int_0^{\frac{1}{k_{\rm B}^2}}\frac{1}{1+x}dx - \int_0^{\frac{1}{k_{\rm B}^2}}\frac{F_{\rm B}(x)}{1+x}dx = \ln\frac{1+k_{\rm B}^2}{k_{\rm B}^2} - \int_0^{\frac{1}{k_{\rm B}^2}} \frac{\pi x}{2M(N_{\rm tA}-w_{\rm A}+1)\Gamma(N_{\rm rB})\bar{\gamma}_{\rm B}(1-k_{\rm B}^2x)} \times \sum_{p=w_{\rm A}}^{N_{\rm tA}}\sum_{m=1}^{M}\frac{\sqrt{1-\phi_m^2}}{B(p,N_{\rm tA}-p+1)}\left(1-\frac{\Gamma(N_{\rm rB},\frac{\psi_{\rm B}x}{1-k_{\rm B}^2x})}{\Gamma(N_{\rm rB})}\right)^{p-1} \times \left(\frac{\Gamma(N_{\rm rB},\frac{\psi_{\rm B}x}{1-k_{\rm B}^2x})}{\Gamma(N_{\rm rB})}\right)^{N_{\rm tA}-p}\left(\frac{\psi_{\rm B}x}{1-k_{\rm B}^2x}\right)^{N_{\rm rB}-1} e^{-\frac{\psi_{\rm B}x}{1-k_{\rm B}^2x}}\frac{1}{1+x}dx. \quad (52)$$

For the convenience in calculating the maximum ADR of the considered system, we assume that the data rates from A to B and from B to A are identical. Therefore, (48) can be rewritten as

$$\mathcal{C} = 2\log_2(N_{\mathrm{tA}}) + 2\int_0^{\infty} \log_2(1+\gamma_{\mathrm{B}}) f_{\gamma_{\mathrm{B}}}(x)dx$$
$$= 2\log_2(N_{\mathrm{tA}}) + \frac{2}{\ln 2}\int_0^{\infty} \frac{1-F_{\mathrm{B}}(x)}{1+x}dx, \quad (49)$$

where $F_{\mathrm{B}}(x)$ is the CDF of $\gamma_{\mathrm{B}}$ given in (43) for the case with TAS. Therefore, the maximum ADR of the considered HI-FD-SM-MIMO system with TAS is presented as (50), as shown at the bottom of previous page.

Since $F_{\mathrm{B}}(x) = 1$ when $x \geq \frac{1}{k_{\mathrm{B}}^2}$, the second integral in (50) is equal to 0. Therefore, the maximum ADR of the considered HI-FD-SM-MIMO system with TAS now becomes

$$\mathcal{C}^{\mathrm{wi}} = 2\log_2(N_{\mathrm{tA}}) + \frac{2}{\ln 2}\int_0^{\frac{1}{k_{\mathrm{B}}^2}} \frac{1-F_{\mathrm{B}}(x)}{1+x}dx. \quad (51)$$

Substituting $F_{\mathrm{B}}(x)$ in (43) into (51), as shown at the bottom of previous page, the integral in (51) is calculated as (52).

Applying the Gaussian-Chebyshev quadrature method [48] to solve the integral in (52), we obtain the maximum ADR of the considered HI-FD-SM-MIMO system with TAS as in Theorem 3. The proof is complete.

## REFERENCES

[1] C.-X. Wang, J. Bian, J. Sun, W. Zhang, and M. Zhang, "A survey of 5G channel measurements and models," *IEEE Commun. Surveys Tuts.*, vol. 20, no. 4, pp. 3142–3168, 4th Quart., 2018.
[2] K. A. Darabkh, O. Amr, H. B. Salameh, and R. T. Al-Zubi, "A–Z overview of the in-band full-duplex cognitive radio networks," *Comput. Commun.*, vol. 145, pp. 66–95, Sep. 2019.
[3] I. Ahmed, H. Khammari, A. Shahid, A. Musa, K. S. Kim, E. De Poorter, and I. Moerman, "A survey on hybrid beamforming techniques in 5G: Architecture and system model perspectives," *IEEE Commun. Surveys Tuts.*, vol. 20, no. 4, pp. 3060–3097, Jun. 2018.
[4] A. H. Gazestani, S. A. Ghorashi, B. Mousavinasab, and M. Shikh-Bahaei, "A survey on implementation and applications of full duplex wireless communications," *Phys. Commun.*, vol. 34, pp. 121–134, Jun. 2019.
[5] M.-T. Le, V.-D. Ngo, H.-A. Mai, X. N. Tran, and M. Di Renzo, "Spatially modulated orthogonal space-time block codes with non-vanishing determinants," *IEEE Trans. Commun.*, vol. 62, no. 1, pp. 85–99, Jan. 2014.
[6] R. Y. Mesleh, H. Haas, S. Sinanovic, C. W. Ahn, and S. Yun, "Spatial modulation," *IEEE Trans. Veh. Technol.*, vol. 57, no. 4, pp. 2228–2241, Jul. 2008.
[7] L. Van Nguyen, B. C. Nguyen, X. N. Tran, and L. T. Dung, "Transmit antenna selection for full-duplex spatial modulation multiple-input multiple-output system," *IEEE Syst. J.*, early access, Jan. 14, 2020, doi: 10.1109/JSYST.2019.2960599.
[8] G. Liu, F. R. Yu, H. Ji, V. C. M. Leung, and X. Li, "In-band full-duplex relaying: A survey, research issues and challenges," *IEEE Commun. Surveys Tuts.*, vol. 17, no. 2, pp. 500–524, 2nd Quart., 2015.
[9] L. V. Nguyen, B. C. Nguyen, X. N. Tran, and L. T. Dung, "Closed-form expression for the symbol error probability in full-duplex spatial modulation relay system and its application in optimal power allocation," *Sensors*, vol. 19, no. 24, p. 5390, Dec. 2019.
[10] B. Jiao, M. Wen, M. Ma, and H. V. Poor, "Spatial modulated full duplex," *IEEE Wireless Commun. Lett.*, vol. 3, no. 6, pp. 641–644, Dec. 2014.
[11] J. Zhang, Q. Li, K. J. Kim, Y. Wang, X. Ge, and J. Zhang, "On the performance of full-duplex two-way relay channels with spatial modulation," *IEEE Trans. Commun.*, vol. 64, no. 12, pp. 4966–4982, Dec. 2016.
[12] S. Narayanan, H. Ahmadi, and M. F. Flanagan, "On the performance of spatial modulation MIMO for full-duplex relay networks," *IEEE Trans. Wireless Commun.*, vol. 16, no. 6, pp. 3727–3746, Jun. 2017.
[13] E. Aryafar, M. A. Khojastepour, K. Sundaresan, S. Rangarajan, and M. Chiang, "MIDU: Enabling MIMO full duplex," in *Proc. 18th Annu. Int. Conf. Mobile Comput. Netw.*, 2012, pp. 257–268.
[14] D. Bharadia, E. McMilin, and S. Katti, "Full duplex radios," *ACM SIGCOMM Comput. Commun. Rev.*, vol. 43, no. 4, pp. 375–386, 2013.
[15] A. Bhowal and R. S. Kshetrimayum, "Outage probability bound of decode and forward two-way full-duplex relay employing spatial modulation over cascaded $\alpha$-$\mu$ channels," *Int. J. Commun. Syst.*, vol. 32, no. 3, p. e3876, 2019.
[16] A. Koc, I. Altunbas, and E. Basar, "Two-way full-duplex spatial modulation systems with wireless powered AF relaying," *IEEE Wireless Commun. Lett.*, vol. 7, no. 3, pp. 444–447, Jun. 2018.
[17] E. Bjornson, J. Hoydis, M. Kountouris, and M. Debbah, "Massive MIMO systems with non-ideal hardware: Energy efficiency, estimation, and capacity limits," *IEEE Trans. Inf. Theory*, vol. 60, no. 11, pp. 7112–7139, Nov. 2014.
[18] A. Papazafeiropoulos, S. K. Sharma, T. Ratnarajah, and S. Chatzinotas, "Impact of residual additive transceiver hardware impairments on Rayleigh-product MIMO channels with linear receivers: Exact and asymptotic analyses," *IEEE Trans. Commun.*, vol. 66, no. 1, pp. 105–118, Jan. 2018.
[19] T. Schenk, *RF Imperfections in High-Rate Wireless Systems: Impact and Digital Compensation*. Dordrecht, The Netherlands: Springer, 2008.
[20] B. C. Nguyen and X. N. Tran, "Performance analysis of full-duplex amplify-and-forward relay system with hardware impairments and imperfect self-interference cancellation," *Wireless Commun. Mobile Comput.*, vol. 2019, p. 10, Aug. 2019.
[21] M. Wen, B. Zheng, K. J. Kim, M. Di Renzo, T. A. Tsiftsis, K.-C. Chen, and N. Al-Dhahir, "A survey on spatial modulation in emerging wireless systems: Research progresses and applications," *IEEE J. Sel. Areas Commun.*, vol. 37, no. 9, pp. 1949–1972, Sep. 2019.
[22] Q. Si, M. Jin, Y. Chen, N. Zhao, and X. Wang, "Performance analysis of spatial modulation aided NOMA with full-duplex relay," *IEEE Trans. Veh. Technol.*, vol. 69, no. 5, pp. 5683–5687, May 2020.
[23] Y. Shao, L. Wang, and X. Cao, "On the performance of space-time block coded spatial modulation transmission for full-duplex relay networks," *IEEE Access*, vol. 7, pp. 180976–180985, 2019.
[24] B. C. Nguyen, T. M. Hoang, and P. T. Tran, "Improving the performance of spatial modulation full-duplex relaying system with hardware impairment using transmit antenna selection," *IEEE Access*, vol. 8, pp. 20191–20202, 2020.
[25] R. Rajashekar, K. V. S. Hari, and L. Hanzo, "Antenna selection in spatial modulation systems," *IEEE Commun. Lett.*, vol. 17, no. 3, pp. 521–524, Mar. 2013.
[26] B. Kumbhani and R. S. Kshetrimayum, "Outage probability analysis of spatial modulation systems with antenna selection," *Electron. Lett.*, vol. 50, no. 2, pp. 125–126, Jan. 2014.
[27] T. Riihonen, S. Werner, and R. Wichman, "Mitigation of loopback self-interference in full-duplex MIMO relays," *IEEE Trans. Signal Process.*, vol. 59, no. 12, pp. 5983–5993, Dec. 2011.
[28] X. Xia, K. Xu, Y. Wang, and Y. Xu, "A 5G-enabling technology: Benefits, feasibility, and limitations of in-band full-duplex mMIMO," *IEEE Veh. Technol. Mag.*, vol. 13, no. 3, pp. 81–90, Sep. 2018.
[29] E. Ahmed and A. M. Eltawil, "All-digital self-interference cancellation technique for full-duplex systems," *IEEE Trans. Wireless Commun.*, vol. 14, no. 7, pp. 3519–3532, Jul. 2015.
[30] P. Zetterberg, "Experimental investigation of TDD reciprocity-based zero-forcing transmit precoding," *EURASIP J. Adv. Signal Process.*, vol. 2011, no. 1, pp. 1–10, Dec. 2011.
[31] T. C. W. Schenk, E. R. Fledderus, and P. F. M. Smulders, "Performance analysis of zero-IF MIMO OFDM transceivers with IQ imbalance," *J. Commun.*, vol. 2, no. 7, pp. 9–19, Dec. 2007.
[32] D. Dardari, V. Tralli, and A. Vaccari, "A theoretical characterization of nonlinear distortion effects in OFDM systems," *IEEE Trans. Commun.*, vol. 48, no. 10, pp. 1755–1764, Oct. 2000.
[33] S. Dey, E. Sharma, and R. Budhiraja, "Scaling analysis of hardware-impaired two-way full-duplex massive MIMO relay," *IEEE Commun. Lett.*, vol. 23, no. 7, pp. 1249–1253, Jul. 2019.

[34] R. Vaughan, N. Scott, and D. White, "Eight hints for making and interpreting EVM measurements," Agilent, Santa Clara, CA, USA, Appl. Note 5989-3144EN, 2005, pp. 1–12.
[35] C. Li, Z. Chen, Y. Wang, Y. Yao, and B. Xia, "Outage analysis of the full-duplex Decode-and-Forward two-way relay system," *IEEE Trans. Veh. Technol.*, vol. 66, no. 5, pp. 4073–4086, May 2017.
[36] A. Jaiswal, M. R. Bhatnagar, and V. K. Jain, "Partially informed transmitter-based optical space shift keying under atmospheric turbulence," *IEEE Trans. Wireless Commun.*, vol. 18, no. 8, pp. 3781–3796, Aug. 2019.
[37] A. Bhowal and R. S. Kshetrimayum, "Outage probability bound of decode and forward two-way relay employing optical spatial modulation over gamma-gamma channels," *IET Optoelectron.*, vol. 13, no. 4, pp. 183–190, Aug. 2019.
[38] W. Wang and W. Zhang, "Huffman coding-based adaptive spatial modulation," *IEEE Trans. Wireless Commun.*, vol. 16, no. 8, pp. 5090–5101, Aug. 2017.
[39] Y. Chen, L. Wang, Y. Ai, B. Jiao, and L. Hanzo, "Performance analysis of NOMA-SM in Vehicle-to-Vehicle massive MIMO channels," *IEEE J. Sel. Areas Commun.*, vol. 35, no. 12, pp. 2653–2666, Dec. 2017.
[40] X. Guan, Y. Cai, and W. Yang, "On the mutual information and precoding for spatial modulation with finite alphabet," *IEEE Wireless Commun. Lett.*, vol. 2, no. 4, pp. 383–386, Aug. 2013.
[41] S.-R. Jin, W.-C. Choi, J.-H. Park, and D.-J. Park, "Linear precoding design for mutual information maximization in generalized spatial modulation with finite alphabet inputs," *IEEE Commun. Lett.*, vol. 19, no. 8, pp. 1323–1326, Jun. 2015.
[42] X. Wang, J. Wang, L. He, and J. Song, "Spectral efficiency analysis for spatial modulation aided layered division multiplexing systems with Gaussian and finite alphabet inputs," *IEEE Trans. Broadcast.*, vol. 64, no. 4, pp. 909–914, Dec. 2018.
[43] A. Jaiswal, M. Abaza, M. R. Bhatnagar, and V. K. Jain, "An investigation of performance and diversity property of optical space shift keying-based FSO-MIMO system," *IEEE Trans. Commun.*, vol. 66, no. 9, pp. 4028–4042, Sep. 2018.
[44] F. Yarkın and I. Altunbas, "Outage performance of spatial modulation with transmit antenna selection over nakagami-*m* fading channels with arbitrary *m*," in *Proc. 8th Int. Congr. Ultra Modern Telecommun. Control Syst. Workshops (ICUMT)*. Oct. 2016, pp. 438–442.
[45] A. Goldsmith, *Wireless Communications*. Cambridge, U.K.: Cambridge Univ. Press, 2005.
[46] A. Jeffrey and D. Zwillinger, *Table of Integrals, Series, and Products*. New York, NY, USA: Academic, 2007.
[47] H. A. David and H. N. Nagaraja, *Order Statistics*, 3rd ed. Hoboken, NJ, USA: Wiley, 2003.
[48] M. Abramowitz and I. A. Stegun, *Handbook of Mathematical Functions With Formulas, Graphs, and Mathematical Tables*, vol. 9. New York, NY, USA: Dover, 1972.

**BA CAO NGUYEN** received the B.S. degree from Telecommunication University in 2006, and the M.S. degree in posts and telecommunications from the Institute of Technology (VNPT), Vietnam, in 2011. He finished the Ph.D. degree course at Le Quy Don Technical University, Hanoi, Vietnam. He is currently a Lecturer with the Faculty of Basic Techniques, Telecommunications University, Nhatrang, Vietnam. His research interests include energy harvesting, full-duplex, non-orthogonal multiple access, spatial modulation, signal processing, and cooperative communication.

**XUAN NAM TRAN** (Member, IEEE) received the M.E. degree in telecommunications engineering from the University of Technology Sydney, Australia, in 1998, and the D.Eng. degree in electronic engineering from The University of Electro-Communications, Japan, in 2003, where he was a Research Associate with the Information and Communication Systems Group, Department of Information and Communication Engineering, from November 2003 to March 2006. He is currently a Full Professor and the Head of the Strong Research Group on Advanced Wireless Communications, Le Quy Don Technical University. His research interests are in the areas of space-time signal processing for communications such as adaptive antennas, space-time coding, MIMO, spatial modulation, and cooperative communications. He is a member of the IEICE and the Radio-Electronics Association of Vietnam (REV). He is a recipient of the 2003 IEEE AP-S Japan Chapter Young Engineer Award, and a co-recipient of two best papers from The 2012 International Conference on Advanced Technologies for Communications and The 2014 National Conference on Electronics, Communications and Information Technology. He is the founding chair and currently the Chapter Chair of the Vietnam Chapter of the IEEE Communications Society.

**LE VAN NGUYEN** received the B.E. degree in electronic and telecommunication engineering, and the M.E. degree in electronics engineering from the Le Quy Don Technical University, Hanoi, Vietnam, in 2008 and 2010, respectively, where she is currently pursuing the Ph.D. degree. Her current research interests include MIMO, spatial modulation, and signal processing for wireless communication systems.

**LE THE DUNG** (Member, IEEE) received the B.S. degree in electronics and telecommunication engineering from the Ho Chi Minh City University of Technology, Ho Chi Minh City, Vietnam, in 2008, and both the M.S. and Ph.D. degrees in electronics and computer engineering from Hongik University, Seoul, South Korea, in 2012 and 2016, respectively. From 2007 to 2010, he joined Signet Design Solutions, Vietnam, as a Hardware Design Engineer. He has been with Chungbuk National University as a Postdoctoral Research Fellow since May 2016. He has more than 50 papers in refereed international journals and conferences. His major research interests include routing protocols, network coding, network stability analysis and optimization in mobile ad-hoc networks, cognitive radio ad-hoc networks, and visible light communication networks. He was a recipient of the IEEE IS3C2016 Best Paper Award.